STRESS CORROSION CRACKING OF 316L AUSTENITIC STAINLESS STEEL IN HIGH TEMPERATURE ETHANOL/WATER ENVIRONMENTS

A Thesis
Presented to
The Academic Faculty

by

Stephani Gulbrandsen

In Partial Fulfillment
of the Requirements for the Degree
Master of Science in the
School of Materials Science and Engineering

Georgia Institute of Technology
June 2012

STRESS CORROSION CRACKING OF 316L AUSTENITIC STAINLESS STEEL IN HIGH TEMPERATURE ETHANOL/WATER ENVIRONMENTS

Approved by:

Dr. Preet Singh, Advisor
School of Materials Science and Engineering
Georgia Institute of Technology

Dr. Arun Gokhale
School of Materials Science and Engineering
Georgia Institute of Technology

Dr. Hamid Garmestani
School of Materials Science and Engineering
Georgia Institute of Technology

Date Approved: June 26, 2012

ACKNOWLEDGEMENTS

I would like to thank my advisor, Dr. Preet Singh, for his encouragement, support, and advice throughout this research project. He provided insight and thought provoking ideas to guide me through the research process. I would also like to thank Jamshad Mahmood for patiently helping me learn test techniques and for regularly helping with the set-up and take down of tests. Sam Raji also deserves thanks and recognition for helping put tests together and take them down. Lindsey Goodman graciously helped me learn my way around the laboratory and provided assistance and advice in preparing tests.

I would like to thank my committee members, Dr. Arun Gokhale and Dr. Hamid Garmestani for their time and insight on my research project. Funding for this project was provided by the Paper Science and Engineering Fellowship from the Institute of Paper Science and Technology. Finally, I would like to thank my parents for their continuous support and encouragement during my time at Georgia Tech.

TABLE OF CONTENTS

LIST OF TABLES

LIST OF FIGURES

Page

LIST OF SYMBOLS

Cl^-	chloride
pHe	pH of a solution containing ethanol
H_2SO_4	sulfuric acid
C	carbon
Mn	manganese
Si	silicon
P	phosphorous
S	sulfur
Cr	chromium
Mo	molybdenum
Ni	nickel
N	nitrogen
Fe	iron
Ti	titanium
Al	aluminum
Pt	platinum
MnS	manganese sulfide
TiO_2	titanium dioxide
MnO	manganese oxide
Al_2O_3	aluminum oxide (alumina)
Cr_2O_3	chromium (III) oxide
NaCl	sodium chloride
Fe_2O_3	iron (III) oxide

LIST OF ABBREVIATIONS

SCC	stress corrosion cracking
EIS	electrochemical impedance spectroscopy
OCP	open circuit potential
SEM	scanning electron microscope
EDX	energy dispersive x-ray spectroscopy
AC	alternating current
SSRT	slow strain rate test

SUMMARY

Interest in the production of bio-fuels and finding a more environmentally friendly pulping process is increasing. Both processes require extraction processes to separate the bio-mass into its constituents, lignin, cellulose, and hemicelluloses. Organosolv delignification is a simple and environmentally benign method that can be used and has been shown to delignify the plant material comparably to traditional kraft pulp processes. Exploratory research has shown that in these high temperature ethanol/water environments stress corrosion cracking (SCC) can occur in 316L austenitic stainless steel.

Experiments were done to understand passive film behavior under static conditions, possible crack initiation sites within the steel, and environmental impact on SCC to draw conclusions about the mechanism. The stability of the passive film over time was studied. It was stable, except Cl^- ions broke through it initiating pits on the 316L surface. The pit initiation sites were found to be MnS stringers, and the pits grew along the pathway of the stringers.

Parametric studies were also conducted to understand the effects of varying water content, temperature, pHe, and Cl^- content for organosolv delignification environments. SCC only occurred in mixed ethanol/water environments that were above water and temperature thresholds and were at an adequate pHe or contained enough Cl^- to destabilize the film.

Results from this study indicate that a film-induced anodic mechanism is like the SCC mechanism, with crack initiation sites dependent on the environment pHe and Cl^-

concentration. Results provide environmental guidelines for organsolv delignification processes for when SCC would not be likely for 316L and when it could become a concern.

CHAPTER 1

INTRODUCTION

1.1 Motivation for Research

The increase in bio-fuels production, particularly bio-ethanol, necessitates an environmentally friendly process that contains few contaminants and a reusable solution. The purpose of the process is to separate the raw materials. Research has shown that approximately 200°C ethanol/water environments, typically acidic with approximately 50 volume % water are promising solutions. These environments, known as organsolv delignification extract lignin, cellulose, and hemicelluloses from plant biomass. They are newly encountered industrial environments and little is known about their SCC behavior on typically adequately corrosion resistant austenitic stainless steels, such as 316L.

Extensive research has been done to characterize the SCC mechanism of 316L stainless steel in aqueous environments, but comparatively little is known about SCC susceptibility of this material in organic solvents. Previous research has indicated that carbon steels in ethanolic environments at room temperature under constant load or slow extension rate test conditions are not susceptible to corrosion in pure ethanol [1]. However, preliminary work has shown that in acidic ethanol/water environments at high temperature SCC can occur, which is only possible in the presence of localized corrosion. This mechanism of SCC is not well understood, and neither are the effects of temperature and pHe and water and chloride content.

1.2 Research Objectives and Technical Approach

The goal of this work is to understand how environmental factors impact SCC of 316L stainless steel in high temperature ethanol/water environments and to propose a mechanism. Specifically the following were studied:

1) The environmental effect on the passive film formation and behavior over time. Immersion tests were done to understand the corrosion behavior of the environments, and electrochemical tests were performed on static 316L test samples to monitor film behavior.
2) The microstructure of 316L was studied to look for anomalies. These features were then related to the localized corrosion behavior of the immersion test samples. Etching was performed to view the microstructure and SEM with EDX was done to analyze the composition at the areas of localized corrosion.
3) The SCC threshold conditions for the following environmental factors: water content, temperature, pHe, and Cl^- content. This data was acquired through slow strain rate tests and microscopic evaluation.
4) Finally, work was done to understand how the water content, temperature, pHe, and Cl^- content impacted SCC when it occurred. Slow strain rate tests were done using a 60 volume % water, 200°C, pHe = 3, 0 ppm Cl^- base to vary these parameters and understand how SCC severity is impacted. The severity was quantified using crack density and velocity, and pit density as appropriate.

With all this information, a SCC mechanism was hypothesized and future work suggestions were made on how to verify this. An understanding of film behavior and

environmental parameters were studied, and are the beginning of characterizing the SCC seen in high temperature ethanol/water environments for austenitic stainless steel.

CHAPTER 2

BACKGROUND

2.1 Industrial Processes Involving Ethanol/Water Mixtures

High temperature ethanol/water environments are used in organosolv delignification processes as an environmentally friendly alternative to kraft pulping [2]. Organosolv delignification requires less steps to clean the pulp, wasting less energy, and it has low levels of sulfur and sodium, suggesting less contamination [2, 3, 4]. This allows for recovery and reuse of cooking liquor as well as production of relatively pure, sulfur free lignin, cellulose, and hemicelluloses. The cellulose and hemicelluloses can be refined into bio-fuels, bio-materials, or pulp and paper. Research has shown that resulting pulp characteristics of organosolv delignification pulp are comparable to similar raw materials pulped by the kraft process, indicating that they are an effective delignification environment [2].

Three factors that affect delignification yields are the ethanol to water ratio, pHe, and temperature. Increasing the ethanol concentration above 50 vol% increases the solids yield, decreases the amount of rejects, and increases the solubilization of lignin, but results in a lowering of water content that demotes lignin cleavage [5]. Pan *et al.* proposed an optimum balance of 65 vol% ethanol to enhance ethanolic processes while not negatively impacting lignin cleavage [5]. These same researchers found that adding 1.35 to 1.5% H_2SO_4 to the ethanol/water mixture results in a maximum solids yield. Above 195°C yields are reduced due to increased solubilization and degradation of hemicelluloses [5].

Researchers have studied these variables to optimize conditions to maximize yield during organsolv delignification. These environments are presented in Table 2.1, where most are approximately 50/50 volume % ethanol/water, slightly acidic, and around 200°C. These conditions, along with chlorides (a possible contaminant), have been proven to promote SCC in 316L austenitic stainless steel, as can be seen in Figure 2.1. 316L is a commonly used material for industrial applications because it is strong and adequately corrosion resistant in most environments. The environment used for testing the 316L sample in Figure 2.1 is comparable to organosolv delignification processes, and stress corrosion cracks can be seen along the sample surface propagating into the material.

Table 2.1: Environmental conditions for optimized organosolv delignification processes.

Process	**Ethanol/Water (vol%)**	**Acidity**	**Temperature (°C)**
Alcell Process [2]	60/40	4.96 - 5.45	195 - 205
Lignol Process [3]	40/60	2 - 3.4	185 - 195
Acidic Delignification [5]	50/50	1.25% H_2SO_4	180
Alkaline Delignification [4]	40/60	0.1% NaOH	180

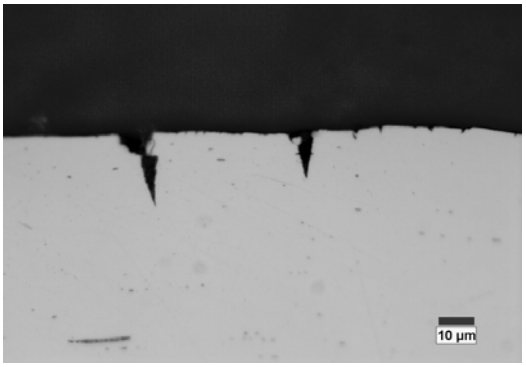

Figure 2.1: Stress corrosion cracks seen along the gage of the sample near the fracture surface for 316L stainless steel in a 60/40 volume % water/ethanol environment at 200°C with pHe = 3.1 and 0 ppm Cl^-.

2.2 316L Stainless Steel Properties and Microstructure

316L is a common austenitic stainless steel known for better corrosion resistance than 304L because of the presence of Mo, which improves the stability of the passive film. It is also cheaper than the more highly alloyed, corrosion resistance Ni-based alloys. Composition and microstructural features of 316L impact the passivation behavior and crack initiation sites. The nominal composition of 316L can be seen in Table 2.2. It is a Fe-based, low C stainless steel with alloying elements to promote corrosion resistance, stabilize the austenitic phase, and maintain adequate strength and ductility. Possible crack initiation sites in 316L are secondary phases, inclusions, and stress induced localized areas of film rupture.

Table 2.2: Nominal composition of 316L austenitic stainless steel.

C	Mn	Si	P	S	Cr	Mo	Ni	N	Fe
0.03	2.00	0.75	0.045	0.03	16.00 18.00	2.00 3.00	10.00 14.00	0.10	Balance

Ni is added to increase impact strength of the steel and stabilize the austenitic phase [6]. The amount added depends on the Mo and Cr contents. Mo and Cr stabilize BCC (ferritic) steel, so enough Ni needs to be included to stabilize the FCC (austenitic) phase [6]. This phenomenon is supported by the Schaffler diagram and Cr and Ni equivalents. The equivalency equations can be seen in Figure 2.2. For 316L the nickel equivalent ranges from 12 to 16, and the chromium equivalent ranges from 19 to 22. This places 316L in the shaded box in Figure 2.2. 316L is on the boundary between austenitic and ferritic stainless steels. Austenitic stainless steels are known for corrosion resistance and ferritic stainless steel are known for strength. Because 316L lies on the edge of these two microstructures, it maintains adequate strength and corrosion resistance.

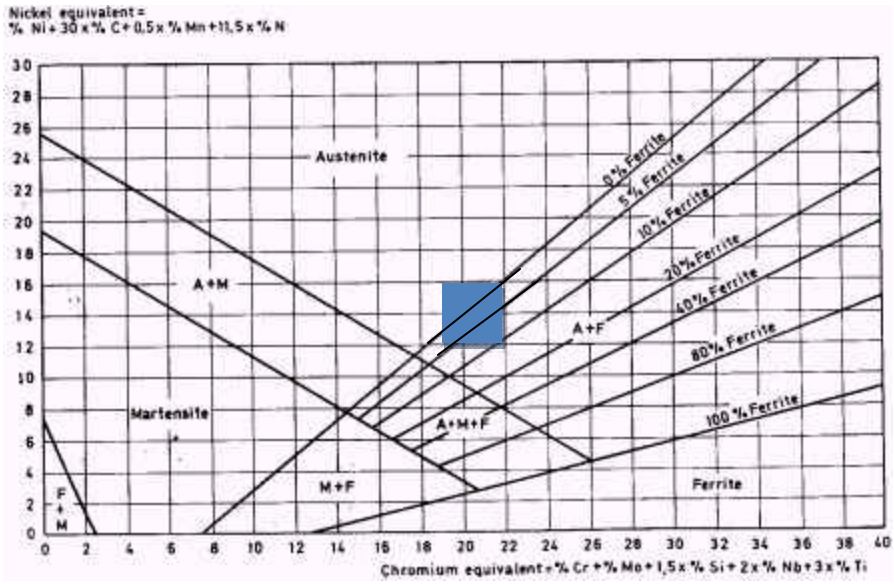

Figure 2.2: Schaffler diagram for microstructure of steels. 316L falls in the shaded blue rectangle on the diagram.

Both molybdenum (Mo) and chromium (Cr) are added to increase corrosion resistance. A minimum of 11 weight % Cr is needed to promote passivation and improve corrosion resistance [7, 8]. As more Cr is added beyond this, the chromium oxide passive film becomes more stable, decreasing corrosion rates [7]. Cr particularly aids in passivation in acidic environments, though the amount of Cr needed depends on the acid type and concentration and the environment temperature [6]. For example, in pure acetic acid 25% Cr is needed for complete corrosion resistance [6].

Like Cr, Mo is added to help increase corrosion resistance of the metal. It increases strength and hardness [7]. Mo increases corrosion resistance of steel in Cl^- containing environments [6, 8]. Cl^- can impair the passivation of 316L, and adding Mo increases resistance to cracking [6, 8]. It is unclear of the exact role Mo plays in increasing corrosion resistance. Mo does not participate in the passive film formation of Cr_2O_3 on the austenitic stainless steels surface [9]. However, it has been proposed that Mo could thicken this existing passive film, increase the surface affinity for oxygen,

which decreases propensity for Cl^- adsorption, or form a more protective secondary film that is a glassy structured amorphous oxide [1]. Whichever of these mechanisms Mo does participate in, only 2 weight % is needed to significantly improve corrosion resistance.

Some additives in stainless steel, like S, Si and Mn, can be beneficial and detrimental to corrosion resistance. S decreases pitting, however once active dissolution occurs it can accelerate this process and poison repassivation [10]. Similarly, Si is added to 316L to reduce pit initiation, however, once pits form Si promotes growth [6]. A concern with adding S is that it can form inclusions, which are anodic relative to the surrounding S-free matrix [11]. The effects of Mn are unclear. Some studies have indicated that it improves pitting resistance up to 10 weight %, but this is only when the Mn remains dissolved in the metal [12]. Unfrtunately, it preferentially reacts with S in the matrix to form Mn S inclusions, which decrease pitting resistance [12, 13]. This is because MnS inclusions are active, particularly in acidic, aqueous, Cl^- containing environments, and they dissolve and form pits on the sample surface [11, 14]. This dissolution creates localized anodic areas on the metal surface, which attract Cl^- ions, promoting pit formation [15]. Sulfide particles can also complex with Ti and Cr, however these sulfides are insoluble and not reactive in aqueous environments, so do not pose a problem to pit initiation [15].

Oxide inclusions are the other type of inclusion common in 316L and they are more stable than sulfide inclusions. They typically contain Cr, Mn, Ti, and Al with a hypothesized TiO_2-MnO-Al_2O_3-Cr_2O_3 structure [11, 14]. These compounds are stable to pH = 3, with the exception of MnO, which is only stable at basic pH, and they do not readily corrode or act as pit initiation sites [14].

Like inclusions, secondary phases can become crack initiation sites in stainless steels. The two types of secondary phases found in 316L are chromium carbides and sigma phase. Sigma phase can be susceptible to corrosion in aqueous, acidic, Cl^- environments [16]. It forms in Mo containing stainless steels between 540 and 1000 °C preferentially at grain boundaries [6]. This impairs corrosion resistance at the grain boundaries by depleting surrounding areas of the film stabilizing Mo [6]. It would be possible to find sigma phase in 316L.

The other type of secondary phase common to stainless steels is chromium carbide $(Fe,Cr)_{23}C_6$, which precipitate at grain boundaries between 425 and 875 °C [6]. Since 316L is being used for this study, it contains less than 0.03 weight % C, which slows the carbide formation reaction down to prevent formation in the above temperature range [6]. As a result, this phase was not present in the materials studied.

2.3 Ethanol/Water Solution Behavior

Material is one important component impacting SCC, and environment in another. Ethanol/water solvents affect the corrosion and SCC behavior differently than pure ethanol or pure water. This is due to the solution behavior that occurs between the two different types of molecules when the solvents are mixed together [17, 18, 19]. It is important to understand how each solution behaves on its' own, as well as what happens when mixed together.

Ethanol, C_2H_5OH, is a polar, protic molecule and the structure of the molecule can be seen in Figure 2.3a. The methyl (CH_3) group on one end of the molecule is nonpolar, while the hydroxyl (OH) group on the other end is polar. Because of this ethanol dissolves polar and nonpolar liquids. Methanol, CH_3OH, is structurally similar to

ethanol, except it has one less carbon atom. A depiction of this molecule can be seen in Figure 2.3b, where the methanol molecule has similar nonpolar and polar properties. Since methanol behaves comparably to ethanol, information on ethanol and methanol was researched to provide information on what is likely happening in ethanol/water environments.

The third molecule of interest, water, is a polar, protic molecule. It does not have a nonpolar region, as can be seen in Figure 2.3c. All three molecules are able to participate in hydrogen bonding with molecules of the same kind and with each other.

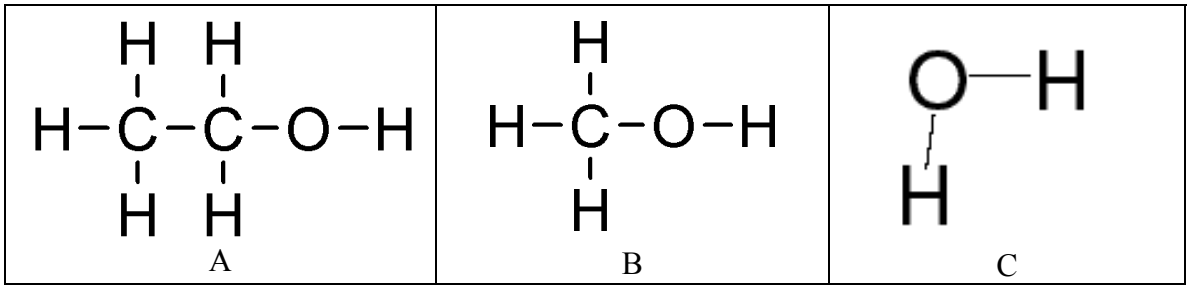

Figure 2.3: Structure of the A: ethanol (left), B: methanol (middle), and C: water (right) molecules.

In ethanol/water systems, water molecules aggregate and show stronger interactions between like molecules than with ethanol molecules [20]. This is substantiated by the work from Dixit *et al.*, who suggested that in alcohol/water mixtures (with methanol/water being the studied system), pockets of hydrogen bonded water molecules exist that take on the typical water structure [21]. Similarly, Parke *et al.* showed that when ethanol is added to water, up to 25 volume% ethanol, the ethanol molecules fill in interstitial spaces in the water molecule matrix [22]. At higher concentrations, linear chains or rings of ethanol form at 20°C and 37°C [22].

Some important molecular properties of ethanol, methanol, and water can be seen in Table 2.3. Ethanol and methanol have comparable densities, which are both slightly

less than water, indicating that in a specified volume, there will be more water molecules than ethanol or methanol molecules. These less dense structures have weaker hydrogen bonding forces holding the molecules together. Another indicator of intermolecular forces and molecule size is the boiling point of the pure liquids. Water has the highest boiling point, while ethanol and methanol boil at lower temperatures. Since the methanol molecule is smaller than ethanol it boils at a slightly lower temperature. The decreased temperature of these two solvents relative to water indicates the intermolecular forces are weaker between the organic solvent molecules.

The next parameter, the dielectric constant, is a measure of the polarity of a molecule, which relates to the solvents ability to separate charges. Water is nearly 3 times as effective as ethanol at separating charges because it is more polar. Methanol falls in between these two, but behaves more like ethanol. The solubility parameter indicates whether two liquids when mixed together will be miscible or immiscible. If the difference between two values is greater than 3, then the two liquids will be immiscible. Both ethanol and methanol are more than 3 points away from water, indicating that the molecules in ethanol/water and methanol/water mixtures prefer to be surrounded by like molecules. Over a wide range of compositions, the solutions are miscible, however the difference in solubility parameters supports the conclusion by Dixit *et al.* that pockets of hydrogen bonded water molecules exist in methanol/water solutions [21].

Another property that could impact SCC is the oxygen solubility in the different environments. It is known that the solubility of oxygen in methanol and ethanol is over ten times greater than the solubility of oxygen in water, indicating that more oxygen will be present in methanol/water or ethanol/water systems than in aqueous environments

[23]. This increase in oxygen content may impact the formation and stability of the passive, oxide-based film that forms on the metal surface.

Table 2.3: Key properties for pure ethanol, methanol, and water.

	Density (g/cm^3)	**Boiling Point (°C) [24]**	**Relative Permittivity ($\varepsilon/\varepsilon_o$) [25]**	**Solubility Parameter (MPa) [25]**
Methanol	0.791	64.7	32.66	29.7
Ethanol	0.798	78.3	24.55	26.1
Water	1.000	100.0	78.30	48.0

To further understand the interactions between ethanol and water at the molecular level and how added NaCl and a Fe_2O_3 surface affect the behavior, Dr. Wonsang Koh performed molecular dynamic simulations [26]. The Fe_2O_3 film is the typical passive layer that forms on carbon steel, however, information on this shows if and how oxide films impact solution behavior. Figure 2.4 shows in a mixture of water and ethanol, water molecules clump together. Figure 2.5 shows when a Fe_2O_3 structure is added to the top and bottom of the simulation box to model the passive film on carbon steel, after 3ns the water molecules preferentially cluster at the oxide surface. Passive films are only able to form on the metal surface in the presence of oxygen, which can be found in air or dissolved oxygen or in water molecules in ethanol/water environments. In order for passivation or repassivation to occur in these environments, the water or oxygen molecules need to be at the metal surface to react with the metal to form a protective oxide film. The water molecules can interact with other polar environmental constituent and solvate them. When the water molecules preferentially migrate to the sample surface, the constituents would come along and become more concentrated at the same surface than in the bulk solution.

To understand this Dr. Koh also studied the effects of adding NaCl on the water cluster size and radial distribution in ethanol/water systems [26]. When added to aqueous solutions, NaCl dissolves into Na^+ and Cl^-, which then interacts with the polar water molecule to form solvated ions. Simulations were run to understand if this interaction impacted the size or amount of water clusters forming in ethanol/water environments. As pictured in Figure 2.6, adding NaCl to the solution did not affect the size of the water clusters [26]. However, it did increase the amount of water clusters, as evidenced by the narrower line seen in the radial distribution function graph.

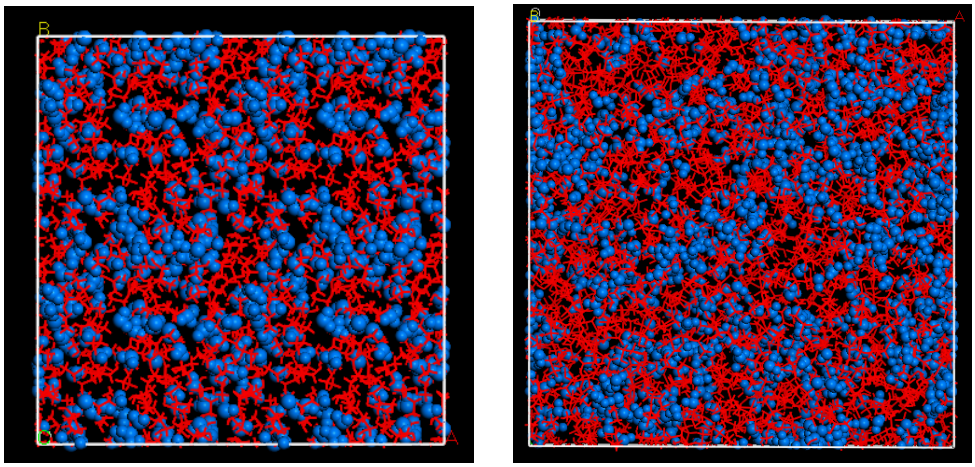

Figure 2.4: Molecular dynamic simulation of 20/80 weight % water/ethanol solution. The initial structure (left) had randomly oriented ethanol (blue) and water (red) molecules, and the final structure (right) showed that the water molecules clump together after the system reaches steady state. [26]

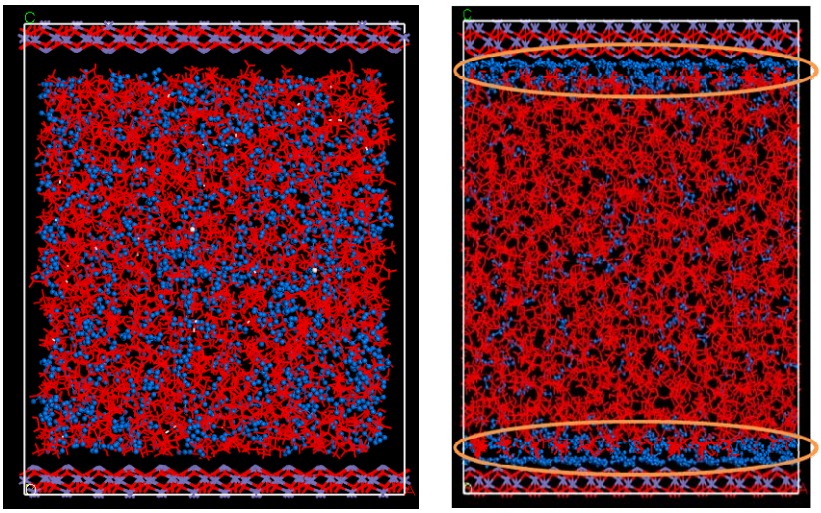

Figure 2.5: Molecular dynamic simulation of 20/80 weight % water/ethanol solution bounded by Fe_2O_3 on the top and bottom. The initial structure (left) had randomly oriented ethanol (blue) and water (red) molecules, and the final structure (right) shows the water molecules congregated at the Fe_2O_3 surface. [26]

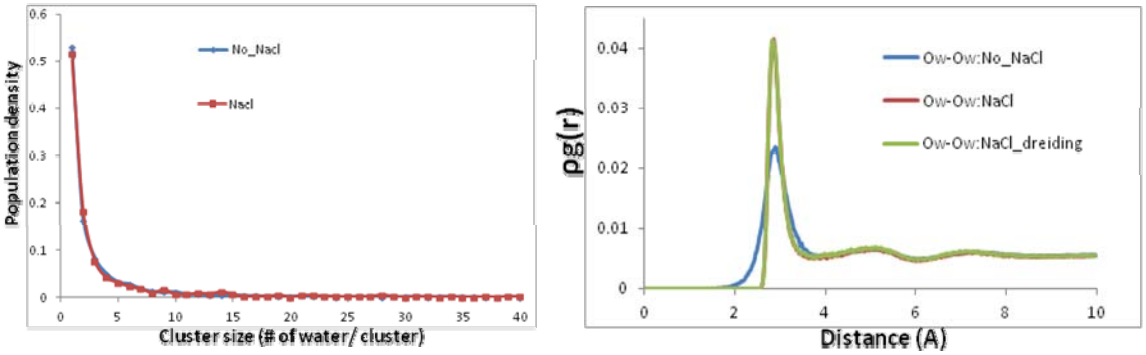

Figure 2.6: Population density graph (left) and radial distribution function (right) for water clusters with and without NaCl in 20/80 weight % water/ethanol solutions. [26]

Therefore, ethanol/water mixtures do not form homogeneous solutions, and the concentration of water molecules at a Fe_2O_3 interface is significantly higher than in the bulk solution. Constituents, such as NaCl, and possibly acids will affect solution behavior, and can become more concentrated at the sample surface, negatively impacting the stability of the passive film.

2.4 Stress Corrosion Cracking Mechanisms

Both material and environment are two key factors that impact SCC. The third, depicted in the Venn Diagram in Figure 2.7 is stress. Only under very specific combinations of these three can SCC occur, and adjusting one of the variables can change the regime from SCC to no SCC or vice versa. The stress in the system needs to be tensile. It can be applied or residual and it causes cracks to form at the surface and propagate through the material. SCC is only possible in selective environments where a passive film forms at the metal surface. Under tensile stresses if the environment is too aggressive and the film formation rate is very slow then general corrosion occurs, and if the rate of surface film formation is very fast then the passive film at the metal surface will immediately repassivate upon rupture [23, 27]. In SCC, the surface is able to passivate, but when the film ruptures the surface of the sample temporarily remains exposed to the environment and locally corrodes.

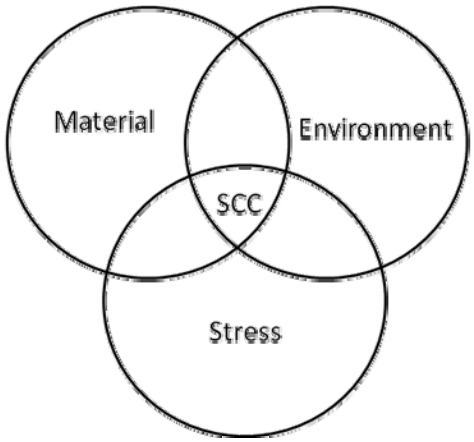

Figure 2.7: Visual representation of the three factors that impact stress corrosion cracking.

Stress corrosion cracks can initiative at abnormalities on the metal surface, including pits, grain or phase boundaries, inclusions, secondary phases, or physical defects such as scratches. Once a crack initiates it can propagate intergranularly or

transgranularly through the microstructure. Crack growth typically occurs when reactions occur faster at the crack tip than on the metal surface or crack sides [27]. Once the crack reaches a critical crack length it continues to propagate through the metal and the remainder of the fracture surface fails.

Table 2.4 lists common SCC mechanisms, identifying how the mechanism works and key fractographic features. Preliminary research in this environment has shown the thumbnail cracks causing failure on the austenitic 316L steel fracture surfaces in high temperature ethanol/water environments are transgranular with crack-arrest marks, indicating discontinuous crack propagation. A representative image is in Figure 2.8, where there is no evidence of voids on the fracture surface. This indicates that of the mechanisms listed in Table 2.4, the most likely mechanisms occurring in the system of study are tarnish-rupture or film-induced cleavage. Because the fracture surfaces have shown transgranular fracture with crack-arrest marks, the film-induced cleavage mechanism is more probable.

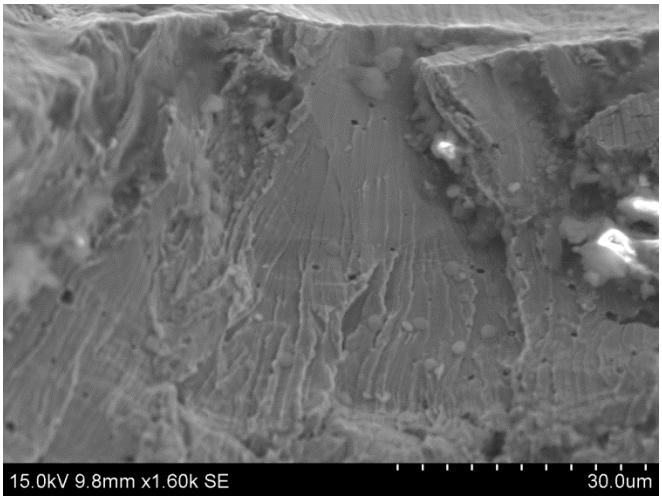

Figure 2.8: Representative SEM image of a thumbnail crack found in a 316L sample. This sample was in a 15 volume % water, 220°C, pHe = 3, 50 ppm Cl^- test environment.

Table 2.4: Accepted stress corrosion cracking mechanisms detailing how cracks initiate and propagate through the metal, as well as key features of the fracture surface. [28]

Type	Title	Mechanism	Fractographic Features
Dissolution	Film-rupture	Stress opens crack and ruptures protective film; tip can remain active or repassivate and rupture by stress or slip steps	• Crack-arrest marks • Intergranular
Dissolution	Active path	Composition difference in microstructure causes dissolution; could be along grain boundary	• Intergranular
Mechanical	Corrosion tunnel	Cracks form at slip steps emerged on metal surface	• Microvoid coalescence on peaks • Grooved fracture surface • Slots • Transgranular
Mechanical	Adsorption-enhanced plasticity (i.e. liquid metal embrittlement)	Chemisorption from environment embrittles metal	• Slip at crack tip • Voids ahead of crack
Mechanical	Tarnish-rupture	Brittle film forms on surface and fractures, exposed metal reacts and reforms film, process repeats	• Transgranular • Intergranular (show crack-arrest marks)
Mechanical	Film-induced cleavage	Film on surface cracks and crack propagates into metal, crack blunts and arrests; tip can remain active or repassivate with repetitive process	• Crack-arrest marks • Discontinuous crack propagation • Brittle cracking in metal • Cleavage-like fracture
Mechanical	Adsorption-induced brittle fracture	Adsorption of environmental species lowers interatomic bond strength and stress needed for cleavage	• Continuous crack propagation
Mechanical	Hydrogen embrittlement	Hydrogen absorbed by metal	• Slip at crack tip • Voids ahead of crack

2.5 Electrochemical Techniques for Stress Corrosion Cracking

Electrochemical techniques, particularly current monitoring and electrochemical impedance spectroscopy (EIS) are useful in understanding the corrosion and passive film behavior of metals in solution. Monitoring open circuit potential (OCP) as a function of time provides information on the activity at the metal/solution interface, assuming the reference electrode is stable and not interfering with measurements [29]. If a reaction is occurring at the metal/solution interface, then the potential will change with time. When the sample surface grows a passive film and becomes less reactive, the potential is expected to gradually increase. If the potential is decreasing, then it would be expected that corrosion is occurring at the interface. A film or corrosion product would be respectively expected on the sample surface upon removal from the environment.

While monitoring OCP provides information on the reactivity, EIS provides kinetic and mechanistic electrochemical information about the system [30]. In EIS, a small AC signal disturbs the working electrode surface, and the electrochemical response is measured [30]. The data is typically presented in the form of Nyquist and Bode plots. Nyquist plots show the real vs. imaginary impedance of the system and are a measure of ohmic resistance with emphasis on series circuit elements [31]. Bode plots display the impedance and phase shift vs. frequency, which is important because the impedance is strongly dependent on the test frequency [31].

Oftentimes, once EIS data is measured, a model circuit can be created to fit the data. The simplest of these model circuits, pictured in Figure 2.9, contains a resistor in series with a capacitor and resistor in parallel. The first resistor from the left represents the solution resistance, the capacitor represents the double layer capacitance or the degree

of film formation, and the second resistor measures the passive film resistance [30, 31]. The model can then be adjusted to fit the data to better understand the kinetic and mechanistic processes of the system.

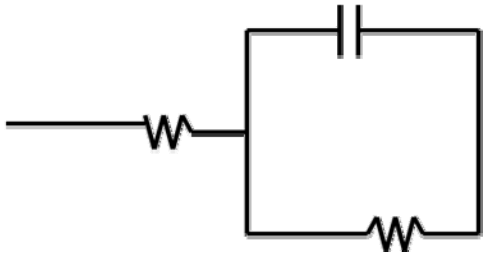

Figure 2.9: A model of a simple circuit that can be used to represent a basic electrochemical system.

Also, similarly to potential measurements, EIS measurements taken for the same system over time can indicate if and how the reactions at the metal/solution interface are changing. An increase or decrease in values seen in the Nyquist and Bode plots would indicate that the kinetics of the chemical reactions are changing with time or that the mechanism of corrosion is changing. Alternately, if the values remain the same with time, then it can be assumed the system is remaining stable.

2.6 Stress Corrosion Cracking Tests

Mechanical testing is crucial to evaluate SCC of a given material in an environment under known stress conditions. When determining the most appropriate test to use to study SCC it is important to look at the sample type, test conditions and constraints, and test set-up. The sample could be smooth or notched, and the test could be under constant strain or constant load and above or below the elastic limit. It is important to understand and take preventative approaches so the test apparatus does not interfere with the test.

The two types of SCC test samples are smooth and notched or precracked specimens. When a sample contains a notch or precrack, the stresses are concentrated at this spot along the sample, increasing the chances for cracking at a known location [32]. If cracking were to occur, it would likely start at the notch or precrack. Also, a precrack provides information on the propensity for a crack to propagate in a given environment [32]. If a crack is already present on a sample surface, when immersed in solution if the environment promotes SCC the crack will grow, whereas if it does not cause SCC the crack will remain the same length.

SCC tests can be held under constant strain or constant load conditions. Most, including slow strain rate tensile tests, bent-beam tests, and U-bend tests have constant strain conditions, while C-ring tests can be under constant strain or constant load [32]. Slow strain rate tensile tests use a tensile dog bone sample that is pulled at an initial strain rate of 10^{-5} to 10^{-7} to accelerate the SCC phenomenon. If the strain rate is too fast, the sample will fracture without SCC because there is not enough time for stress corrosion cracks to initiate on the surface [32]. As cracks grow, the applied stress decreases because the load bearing area decreases [32].

In bent-beam tests, a rectangular sample is placed in a 2-,3-, or 4-point loaded sample holder that curves the sample introducing constant strain. The sample and holder are placed in the test environment. These tests only test stress levels below the elastic limit for the sample and multiple samples can be placed in the same environment at the same time [32]. In all three sample holders, the maximum stress occurs at the midpoint of the convex surface and there is zero stress at the ends of the sample in the holder [32]. Of the three options, the 4-point loader is preferred because it creates uniform longitudinal

stress on the convex surface [32]. The 3-point loader can introduce extra pressure at the center due to the central support.

U-bend tests, the third type of constant strain test, consist of a rectangular bar specimen bent 180° into the shape of a U and placed in the test environment. The stress conditions of the sample are unknown, and only ductile samples that do not crack with bending can be used [32]. These samples are typically in a high stress state that cause quick crack propagation [32].

The final type of test, C-ring tests, can be constant load or constant strain conditions. For this test, a C-shaped specimen is machined from the sample, and a screw is placed between the two ends of the C and tightened to produce the desired test conditions [32]. Once the sample is prepared it is placed into the test environment.

Of these tests, only the slow strain rate test will definitely fail and it takes the shortest amount of time. The time will be less than or equal to the time it takes the material to fail in an inert environment. The other three tests require periodic visual analysis of the samples to look for crack initiation. Oftentimes, this includes interrupting the test, removing the sample from the environment, visually analyzing it, then returning it to the environment if no cracks are present. These tests can last on the order of 5-10 weeks, though multiple samples can be placed in the same test environment.

In slow strain rate tests the sample is not loaded until after it comes in contact with the environment. The sample can be preloaded with stress once it is set up in the test apparatus. The bent-beam, U-bend, and C-ring tests are typically put in the sample holder and then placed in the test environment. The samples are stressed initially outside of the test environment, which could impact SCC behavior. Finally, it is important in all test

set-ups to pay attention to the occurrence of crevices and the potential for galvanic corrosion caused by the sample holder.

Of the types of tests listed, slow strain rate tensile tests are the preferred test because they take less time (although that means the SCC process is accelerated) and the sample does not experience any types of stress until placed in the test environment. The test apparatus holds the ends of the specimen and does not come in contact with the narrow region of the specimens that experience the highest stress, making it less likely for crevices to occur. Depending on the test set-up, it is possible to only expose the gage length of the sample to the test environment, which would eliminate the potential for galvanic corrosion.

2.7 Stress Corrosion Cracking in Ethanol/Water and Methanol/Water Systems

Now that the material, test environment, electrochemical monitoring, and SCC mechanism and test methods have been explored, it is important to understand what is already known about SCC for alcohol/water environments. The effects of the four constituents: water content, pHe, Cl^-, and temperature were studied to understand what is already known to occur in these systems.

2.7.1 Water Effects

It has been noted that in protic alcohols, like ethanol, water content influences passivation behavior and affects if and when the active to passive transition will occur in the system [17, 33]. Gallo and Edmondson define a passive film as "the formation of a corrosion product on the surface [of a metal] that resists further corrosion in an environment" [9]. For 316L in air and aqueous environments, the film is non-porous Cr_2O_3 1-3 nanometers thick [9]. It forms from Cr in the metal reacting with oxygen from

the atmosphere. Oxygen can be supplied from the air or dissolved in the environment or from water molecules in a water-containing environment. Cr_2O_3 is a very stable film because upon exposure to oxygen, the film immediately forms to protect the sample surface from further corrosion.

Under tensile stresses, such as in slow strain rate tests, it is possible for the film to break. The only way it can reform is if oxygen is present in the system. The oxygen can be dissolved in the water or come from the water. This is why water is so important to ethanol/water systems because the water can provide oxygen to allow the film to reform locally where it has broken to continue protecting the sample surface. When the film is unable to reform, the local cracks can become initiation sites for SCC.

Depending on the other constituents and their concentrations, as well as the metal surface in question, different concentrations of water are needed to cause a passive film to form. In a methanol/water system at room temperature, Singh *et al.* found that the most beneficial water content for corrosion resistance was between 0.5 and 1.5 volume %, below 0.5 volume % and above 1.5 volume % an unstable or poorly protective passive film formed [34]. Tajima *et al.* were studying the propensity for pitting in organic acid/methanol systems and found that water in the system inhibited the ability for pitting to occur [35]. It is suspected this inhibition they mentioned is the more stable passive film that forms because water molecules are present and able to keep it stable. To prevent this effect and allow for pitting, very low (unspecified quantity) water contents were used and pitting was found [35]. This supports the hypothesis that water does impact passive film formation and behavior in ethanol or methanol/water environments.

Similar to methanol/water systems, ethanol/water systems also show a threshold water content for surface passivation at room temperature. In an acidic ethanol/water/hydrochloric acid solution, 304 austenitic stainless steel only passivated at water contents greater than 10 volume % [17]. Sekine *et al.* looked at the surface topography for 430 stainless steel samples in acidic aqueous ethanol, and found that increasing the water concentration caused a more uneven sample surface because the film was thinner and less stable at higher water contents [36]. In this test as the water content increased the corrosion rate for the sample also increased due to the film stability [36].

As Newman *et al.* stated, in alcoholic environments for carbon steels it is likely the impurities in the alcohol that induce stress corrosion cracking [23]. He reviewed the literature to understand the SCC mechanism of carbon steel in alcohols and found that alcohol/water environments behave differently than pure alcohol, but a third constituent such as acetic acid is necessary to promote SCC, as water is not solely responsible for inducing SCC in these environments [23]. Even though the water content may not impact the propensity for SCC, it has been shown to effect the formation and stability of the passive film on the metal surface.

It is important to pay attention to the water content in the environment. Because ethanol and methanol are hygroscopic the water content environment can increase, potentially affecting the stability of the passive film.

2.7.2 pHe Effects

Adding a third constituent to alcohol/water environments such as acid has been shown to affect film formation and corrosion behavior. In a methanol/water system acidified with H_2SO_4, 304 showed a more stable passive film as the acid content

decreased (i.e. pHe increased) [34]. In this same system when the H_2SO_4 content decreased, the critical potential for passivity became more noble, indicating an increase in the stable passive range for the solution [34].

In an ethanol/water system acidified with sulfuric acid, increasing acid content increased metal dissolution (i.e. general corrosion) for 304 stainless steel because the passive oxide film was destroyed [33]. This behavior was also seen in a simulated fuel grade ethanol environment at room temperature for carbon steel, where increasing the acidity of the system increased general corrosion [37]. Similarly, Castle *et al.* in a neutral 3.5% aqueous NaCl solution for 316 showed increased dissolution at the metal surface with acidic pH, but inhibited corrosion at neutral and basic pH [11].

Tajima *et al.*, Lou *et al.*, Singh *et al.*, and Singh *et al.* showed that in acidic organic solvent environments at room temperature acidic pH can promote pitting on the metal surface [33, 34, 35, 37]. This behavior was seen for 304 stainless steel in acetic acid/methanol solutions, in simulated fuel grade ethanol environments with carbon steel, in H_2SO_4/methanol environments with 304, and in H_2SO_4/ethanol environments with 304 at room temperature [33, 34, 35, 37]. In multiple systems, higher acid concentrations (i.e. lower pH) showed more severe pitting and a higher density of larger pits [33, 34].

As before, Newman stated impurities in alcohol, including acidity (and not just water content) are likely responsible for SCC in carbon steel in alcohol environments [23]. Research has shown that the pHe of the environment affects the passivation behavior of the surface and the corrosion susceptibility. Acidic pHe destabilizes the passive film on the sample surface, so when it is destroyed it is more difficult to reform. The longer the base metal is exposed to solution without a passive film, the longer the

corrosive environment is in contact with the sample surface, which can cause a crack to form on the sample surface.

2.7.3 Chloride Effects

Like acidic pHe, Cl^- affect the pitting behavior of stainless steels in organic solvent/water solutions. Little research has been done to understand the effects of Cl^- in these environments. However, Cl^- are known to promote SCC in aqueous environments for austenitic stainless steels. For carbon steel in alcoholic environments, Cl^- in the range of tens of ppms can change the fracture mode from intergranular to transgranular [23]. Cl^- ions are aggressive halide ions that will initiate cracks via pit formation on the surface of stainless steel [27]. Beyond this, as the Cl^- content is increased, the tendency for pitting also increases [38].

Cl^- ions preferentially initiate pits at S-rich inclusions, particularly MnS inclusions [10, 11, 15]. Cl^- ions adsorb to the S inclusion, causing the inclusion to dissolve and act as a local anode [11]. After the inclusion dissolves the metal surface should repassivate, but if a Cl^- or salt film forms where the pit had been this can lead to pit propagation, especially if there is a locally increased concentration of Cl^- within the pit [15]. The dissolution of S inclusions is potential dependent, and Stewart *et al.* has shown that this can occur at the measured potentials on a passive surface [10].

Cl^- are not a constituent included in the environments for organosolv delignification processes, as can be seen in Table 2.1. They can become a contaminant during the process, either from earlier process streams in the pulping process or from the raw material (wood chips), which is why it is important to understand their impact in ethanol/water environments.

2.7.4 Temperature Effects

As can be seen from the research presented thus far, most of the work in ethanol/water systems has been conducted at room temperature. The environments in Table 2.1 are at elevated temperatures between 100°C and approximately 200°C. Hongzhang *et al.* noted that the two most important factors in yields for delignification were time and temperature [4]. They created a severity factor based on these two variables and found that of all the environmental variables, as the severity factor increased, then so did the delignification [4]. However, the effects of increased temperature on the SCC behavior of austenitic stainless steels in organosolv process related environments is not very well known.

It is possible that the solution behaves differently at higher temperatures. Research has shown that between 200°C and 400°C alcohols can experience catalytic oxidation, in which the C-C bond in ethanol can be cleaved [23]. This typically occurs over ferric oxide or mixed oxide surfaces containing ferric ions [23]. The reaction products are carbon dioxide and water [39]. If this reaction is catalyzed by an oxide layer, like the passive film, then the water content at the metal surface would be greater than in the bulk concentration. It has already been discussed that water content affect passive film stability. The exact impact of temperature as well as the passive film composition on the ethanol catalyst reaction is not well known for water/ethanol environments with varying water concentration.

2.8 Summary

Organosolv delignification processes are high temperature ethanol/water environments that have been shown to promote SCC in 316L austenitic stainless steel.

316L is typically a corrosion resistant material because it contains Cr and Mo, where the Mo stabilizes the Cr_2O_3 passive film that forms on the surface of the material, protecting it from corrosion. Secondary phases, like MnS inclusions, could act as crack initiation sites by promoting localized corrosion of the material.

When ethanol and water are mixed together, the water aggregates at the oxide surface, which can facilitate concentration of destabilizing environmental constituents, such as Cl^-, at the metal surface. Water and pHe have been shown to impact stability of the passive film, while Cl^- and pHe can promote pitting on the sample surface. Temperature can cause a reaction of the ethanol over the metal oxide, which may impact SCC susceptibility. A mechanical, film-induced cleavage SCC mechanism is expected based on preliminary results and will be tested using slow strain rate tests because they are the most controlled SCC tests. Despite this knowledge, there is still much to learn about the behavior, mechanism, and environmental impact of water, pHe, Cl^-, and temperature on SCC of 316L in high temperature ethanol/water environments.

CHAPTER 3

EXPERIMENTAL APPROACH

3.1 Material Selection

316L was chosen as the test material because it is a cost effective, adequately corrosion resistant stainless steel commonly used in industrial applications. It would likely be used for manufacturing reaction vessels for organosolv delignification processes. The nominal composition for 316L is presented in Table 3.1. Mo and Cr aid in the corrosion resistance, while Ni increases strength. The L denotes < 0.03 weight % C to prevent chromium carbide formation.

Table 3.1: Nominal composition of 316L stainless steel.

C	Mn	Si	P	S	Cr	Mo	Ni	N	Fe
0.03	2.00	0.75	0.045	0.03	16.00 18.00	2.00 3.00	10.00 14.00	0.10	Balance

Some typical mechanical properties of 316L are presented in Table 3.2. Comparable mechanical properties were seen in the tensile tests. These values indicate that 316L is a strong material, yet able to be machined into test specimens.

Table 3.2 Mechanical properties of 316L stainless steel.

Tensile Strength (MPa)	Elastic Modulus (GPa)	Yield Strength, 0.2% Proof (MPa)	Rockwell B Hardness	Density (g/cm^3)
485	193	170	95	8.00

3.2 Coupon Exposure Tests

To understand the corrosion behavior of 316L stainless steel in high temperature ethanol/water environments, coupon exposure tests were run in conjunction with slow strain rate tests. Figure 3.4a shows three test coupons polished to 2000 grit resting on the bottom of the slow strain rate test load-train. They were submerged in solution and

exposed for as long as the slow strain rate test took to fail, which varied from 24-48 hours. After testing, the samples were analyzed with optical microscopy for evidence of corrosion. If pits were found on the surface, they were characterized by morphology and pits per unit area on the sample were calculated. Many of the pits found were long and worm-shaped. Since it was difficult to deduce how many circular pits these formed from, they were counted as one. Two worm-shaped pits nearby each other on the surface were counted separately if they were not visibly connected. Pit composition was further imaged and analyzed using a Hitachi S-3700N Variable Pressure scanning electron microscope with energy dispersive x-ray spectroscopy.

Film removal and corrosion rates were calculated for each test environment. The film was removed using a light (approximately 10 psi) sand blast on the sample surface for less than 5 seconds. The time used to calculate the corrosion rate was the duration of the slow strain rate test, which was turned on when the autoclave reached environmental temperature and stopped when the temperature was turned off after sample failure.

3.3 Electrochemical Tests

Electrochemical tests were used to understand the surface activity on 316L stainless steel samples exposed to SCC inducing high temperature ethanol/water environments. These tests were performed using a three electrode set-up, pictured in Figure 3.1. The working electrode was the 316L test specimen, a Pt mesh was used for the counter electrode, and a Pt foil was used as a quasi-reference electrode. A Pt quasi-reference electrode was chosen because it could withstand the autoclave pressure and the test environment and it eliminated the potential for solution contamination by Cl^- from a salt bridge [40]. It was assumed that since the test was occurring in the sealed autoclave,

the environment was not changing during testing and variations seen in the data were from the working electrode and not the inert Pt electrode.

Potential monitoring along with electrochemical impedance spectroscopy (EIS) were performed for cylindrical static 316L samples using a Gamry Reference 600 potentiostat. Open circuit potential (OCP) was monitored for one to two days after the environment reached the set temperature to determine how the film behaved statically over time. Periodically, EIS was run on the sample to gather more evidence on film behavior. Due to the low conductivity in the environments, it was difficult to get data below a frequency of 10,000 Hz.

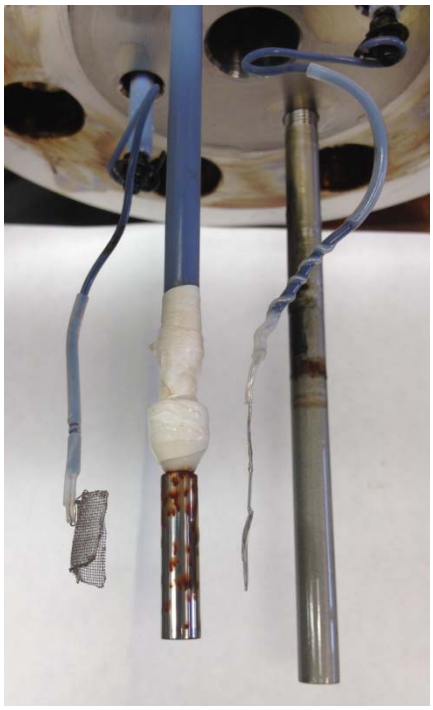

Figure 3.1: Three electrode set-up used in static electrochemistry tests. The electrodes (from left to right): Pt mesh counter electrode, cylindrical 316L stainless steel working electrode, Pt foil quasi-reference electrode, thermocouple sleeve.

The electrochemical data was used to characterize the film behavior under static conditions. Three environments were tested; all contained 60 volume % water and were

at 200°C. One had a low pHe of 3 and 0 ppm Cl^-, the next had a pHe of 6 and 50 ppm Cl^-, and the third had a pHe of 3 and 50 ppm Cl^-. The OCP data and EIS data was compared between environments to better understand how each constituent impacts the static film, and what happens when both acid and Cl^- are added to the system in SCC inducing concentrations.

3.4 Metallographic Analysis

The microstructures of extruded rod and sheet 316L stainless steel samples were analyzed for grain size and inclusion characterization. Inclusions or secondary phases were quantified as they can act as crack initiation sites. Multiple sections from tested slow strain rate test samples were analyzed to ensure uniformity of the microstructure across samples. Only one immersion test sample was used because all of these specimens come from the same 316L sheet.

Rod samples were mounted to expose the longitudinal and transverse faces, whereas sheet samples were mounted to examine the microstructure in all three directions (i.e. longitudinal (rolling direction), transverse, and short-transverse).Samples were mounted and polished up to 0.05 μm alumina powder finish. Then they were electroetched at 6 V DC in 10% oxalic acid solution for 55 seconds. Optical microscopy was used to systematically image the samples, taking 6 fields of view from every mounted sample. ASTM E 112-10 was used to quantify grain size and ASTM E 45-05 was used to characterize inclusions.

The following equation was used to calculate grain size:

$$G = (6.643856\log_{10}\check{N}_L)-3.288$$

where G is ASTM grain size number and $\check{N}_L$ is the number of grain boundary intersections per mm. The ASTM standard details that the volume fraction of an inclusion can be estimated using point counting with the following:

$$\text{Volume fraction of inclusion} = \frac{V(\text{inclusions})}{V(\text{sample})} = \frac{\text{Points on an Inclusion}}{\text{Total Points in the Grid}}$$

Grain size measurements were taken longitudinally and vertically across images to determine if the grains were elongated. Volume fraction of the inclusions was done using a 16 point grid on each field of view, and inclusion characterization was done on fields of view that showed stringers. They were quantified using lines running perpendicular to the stringers. Figure 3.2 shows the placement of the test lines on the fields of view.

To characterize the inclusions, Method B (Length) was used. The data is reported in the following manner (Longest Stringer)$^{\text{thickness}}{}_{\text{connectedness}}$-(Average Length of Remaining Stringers)$^{\text{Number of stringers averaged}}$. Stringer lengths are only reported as whole numbers based on how many spacer lines, pictured in Figure 3.2B they span. The lengths are round down, for example if a stringer is longer than one spacer, and not quite two, it is counted as one unit long.

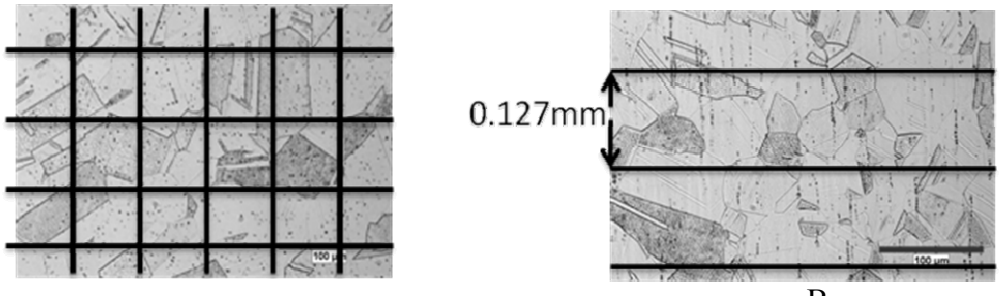

A B

Figure 3.2: A: Representation of the test lines used for calculating grain size and the grid created by the intersection of these lines was used to calculate inclusion volume fraction. B: Representation of test lines used to characterize severity of inclusions.

3.5 Slow Strain Rate Tests

Slow strain rate tests are tensile tests that accelerate the phenomenon of SCC and are used to determine environmental conditions under which a given material could be susceptible to SCC. Cylindrical dog-bone specimens, shown in Figure 1, were machined out of ¼" 316L rod. These samples had a gage length of 15 mm and a gage-diameter of 3 mm.

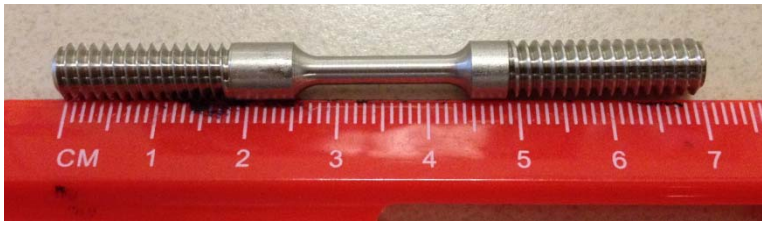

Figure 3.3: Slow strain rate test sample used in slow strain rate tests.

Samples were mounted in the load-train shown in Figure 2A, then immersed in solution in a DSS 2205 autoclave and sealed for the duration of the test. An initial strain rate of 1.3×10^{-6} s^{-1} was applied, and straining did not commence until the environment reached the set temperature. Tests lasted approximately 24 - 48 hours until the sample fractured.

A B

Figure 3.4: A: Sample mount for the slow strain rate tests. B: Sealed autoclave during a slow strain rate test.

Upon fracture, the autoclave was cooled and the two halves of the tested sample were removed and stored in a desiccator. Samples were analyzed with optical microscopy and the % elongation and % reduction in area were calculated. One half of the tested samples was mounted and polished to 0.05 μm alumina powder finish, and used to quantify the extent and mode of SCC. Cross sections of the samples were imaged with optical microscopy and, if cracking occurred, characterized via crack density and crack velocity.

Crack density was calculated averaging the number of cracks of all lengths on both sides of the mounted sample cross section that occurred between the fracture surface and 1 mm away from it. Crack velocity was calculated by measuring the deepest crack visible on the cross section and dividing it by the time to failure of the sample. These measurements were used to compare SCC severity.

CHAPTER 4

CRACK INITIATION: CORROSION AND MICROSTRUCTURE ANALYSIS

The role of microstructure and the passive film formed at the surface of 316L stainless steel on the corrosion behavior were investigated. The focus was to understand how localized corrosion may impact stress corrosion crack initiation, and if microstructural features promote localized corrosion. Immersion tests were performed and analyzed for evidence of localized corrosion and the microstructure of these samples was etched and studied for possible crack initiation sites.

4.1 Corrosion Rate in Ethanol/Water Environments

Coupon exposure tests lasted 1-2 days and were performed in conjunction with slow strain rate tests. These tests were shorter than typical 10-15 day exposure tests, but were able to show evidence of the corrosion behavior of 316L stainless steel in ethanol/water environments. The coupon exposure tests in most environments tested did not show significant corrosion of 316L stainless steel. With the exception of two samples the remaining stainless steel samples had corrosion rates less than 0.42 mils per year (mpy). This data is shown in Table 4.1, where the most significant corrosion rate was 1.09 mpy for a Cl^- containing environment. Overall, the highest corrosion rates were seen at or above 175°C.

Table 4.1: Corrosion rate data arranged from largest to smallest rate.

Water (vol %)	Temperature (°C)	pHe	Cl^- (ppm)	Corrosion Rate (mpy)	Pitting?
60	200	5.8	30	1.088	Yes
50	200	6.4	0	0.647	No
15	200	2.6	0	0.414	No
60	200	5.8	10	0.360	Yes
90	150	3	30	0.341	No
60	220	6	100	0.305	No
60	175	6.2	50	0.286	Yes
1	200	6.3	30	0.270	No
60	220	3.1	0	0.234	No
10	175	4.3	20	0.233	No
60	200	2.5	0	0.192	No
15	220	3.2	50	0.148	No
60	200	6	0	0.136	No
10	200	3.2	100	0.121	No
15	100	3.2	0	0.119	No
90	150	2.4	10	0.102	No
1	100	3.2	10	0.072	No
60	200	4.2	0	0.070	No
1	200	8	0	0.069	No
60	200	5.9	5	0.043	Yes
60	200	5.9	50	0.000	No
30	100	8.2	30	0.000	No
90	200	3.1	0	0.000	No
1	220	4	20	0.000	No
100	200	5.8	0	0.000	No
0	200	6.1	0	0.000	No
70	200	6.5	0	0.000	No
60	200	3.1	0	0.000	No
60	200	4.8	0	0.000	No
60	150	3.1	0	0.000	No
60	150	3.1	0	0.000	No

The effect of temperature on corrosion rate is presented in Figure 4.1. Corrosion is only seen at 220°C for a 60 volume % water, pHe = 3, 0 ppm Cl^- environment, with a general trend of corrosion rate increasing as temperature increase. Cl^- content shows a similar trend in Figure 4.2, where corrosion rate increases with Cl^- content for 60 volume

% water, 200°C, and pHe=6. When the Cl^- content is double, the corrosion rate increases 10-fold, and when the Cl^- content is tripled, the corrosion rate increases 3-fold. A more significant increase in corrosion rate is seen at lower increases in Cl^- concentration. It is expected that the corrosion rate will continue increasing with added Cl^-, just at a lower rate.

Water content shows a peak in corrosion rate in Figure 4.3 at 50 volume % for 200°C, pHe=6, and 0 ppm Cl^-. It then drops off on either end. This indicates max corrosion occurs around this value, gradually increasing from 0 volume % water, with a significant drop in corrosion rate by 60 volume % water. Figure 4.4 shows no obvious trend for pHe, with a slight inclination toward more corrosion at lower pHe. The highest corrosion rate was seen at pHe = 2.5, but there is also a spike around pHe = 4. This corrosion rate at pHe = 4 is less than half of the maximum corrosion rate seen at pHe = 2.5.

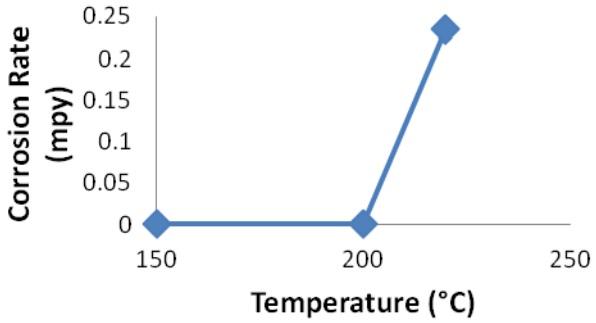

Figure 4.1: Temperature effects on corrosion rate for 60 volume % water, pHe = 3, 0 ppm Cl^-.

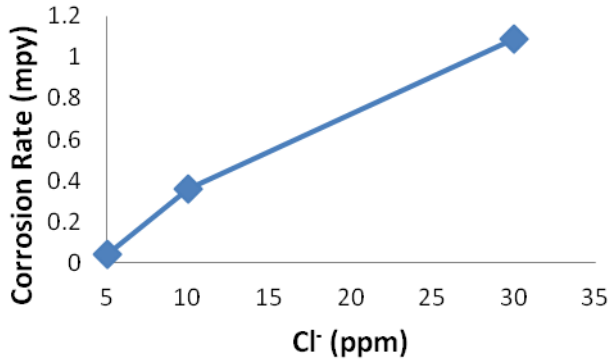

Figure 4.2: Cl^- effects on corrosion rate for 200°C, 60 volume % water, pHe = 6.

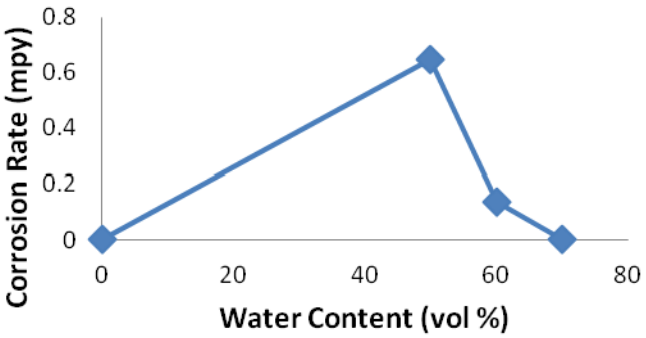

Figure 4.3: Water content effects on corrosion rate for 200°C, pHe = 6, 0 ppm Cl^-.

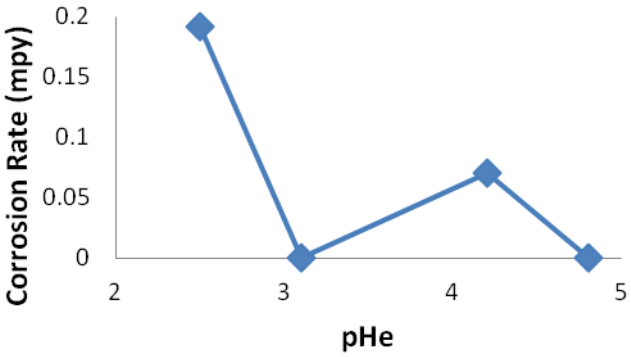

Figure 4.4: pHe effects on corrosion rate for 200°C, 60 volume % water, 0 ppm Cl^-.

Of these variables, Cl^- and water most impact corrosion rate because they have the largest values. It would be expected that the highest corrosion rate would occur around 50 volume % water, 220°C, pHe = 3.5, and 100 ppm Cl^- given the ranges of the variables tested. Overall, the corrosion rates are very small and indicate corrosion is not a concern in these environments. This can imply that under static conditions, the passive film on the

316L stainless steel surface is stable and adequately protects the bulk material from environmental attack.

4.2 Electrochemical Characterization of Passive Film Behavior

To better understand how the film behaves with time in a static environment, the electrochemical behavior was monitored to look at how film stability changed with time. The three tests looked at the impact of being below the pHe threshold, being above the Cl^- threshold, and the combined effects of both parameters.

OCP and EIS of 316L cylindrical samples in select SCC inducing environments showed inactive static film behavior for 1 to 2 days. Table 4.2 indicates the three test environments used, and Figure 4.5 shows how potential varied with time for these three environments. The points on the OCP data indicate the times at which EIS was run.

Table 4.2: Environments used in electrochemical monitoring of film behavior for static tests.

Environment	**Water Content (volume %)**	**Temperature (°C)**	**pHe**	**Cl^- (ppm)**
Low pHe	60	200	3	0
High Cl^-	60	200	6	50
Low pHe and High Cl^-	60	200	3	50

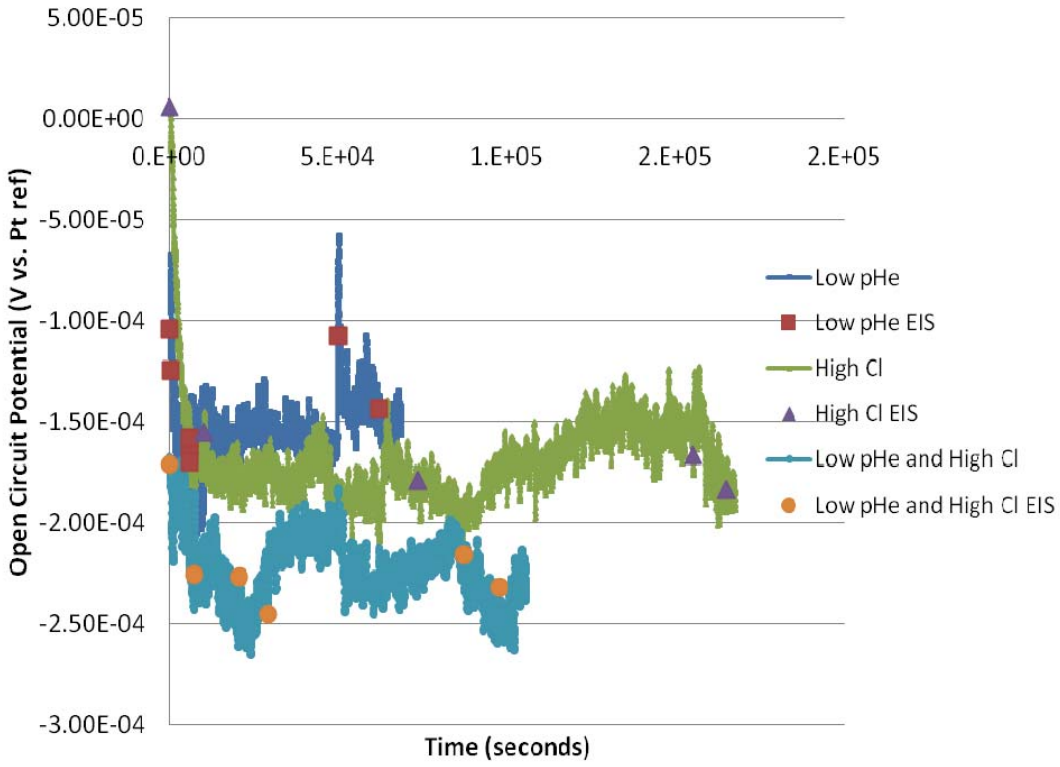

Figure 4.5: Open circuit potential measurements for 316L stainless steel in the three environments listed in Table 4.2. Potential was taken relative to a Pt foil quasi-reference electrode.

The OCP data shows that both the low pHe and high Cl^- environments began at a potential positive of the static potential, then dropped down to the static value. However, the variations seen during the OCP measurements are very small (on the order of tenths of millivolts), indicating that electrochemical potential is almost static. This further indicates the surface film or surface activity did not change over time.

Visual examination of the 316L stainless steel samples upon removal from the test environment revealed the low pHe sample did not show any evidence of corrosion, however the high Cl^- sample had one small pit initiation site on the surface, and the sample exposed to a low pHe and high Cl^- solution had numerous pits on the sample surface. OCP measurements did not show this difference in corrosion behavior, possibly

because these perturbations due to local corrosion attacks were so small relative to the total sample surface that they were difficult to pick up with the electrochemical data.

The Bode and Nyquist plots for each test environment are presented in Figures 4.6, 4.7, and 4.8. Figure 4.9 compares the last EIS run of all three environments. The data in Figures 4.6, 4.7, and 4.8 shows that as time progresses (EIS run number increases) the electrochemical behavior of the sample in tested environments, including the film properties remains the same, as is shown in Figures 4.6 to 4.8 by the overlapping data points from the different test times. This further supports the notion that in a static environment, the passive film is not affected by the environment. Rather, a tensile stress needs to be applied to the sample to rupture the film and allow cracks to form. This also suggests that the SCC mechanism in the system may be film-induced. This holds true for the acid only environment, however added Cl^- can locally rupture the film and form pits, which when occurring in conjunction with tensile stress can cause cracks to form and propagate. The cylindrical specimens were not experiencing tensile forces, so the pits formed, but did not grow into cracks.

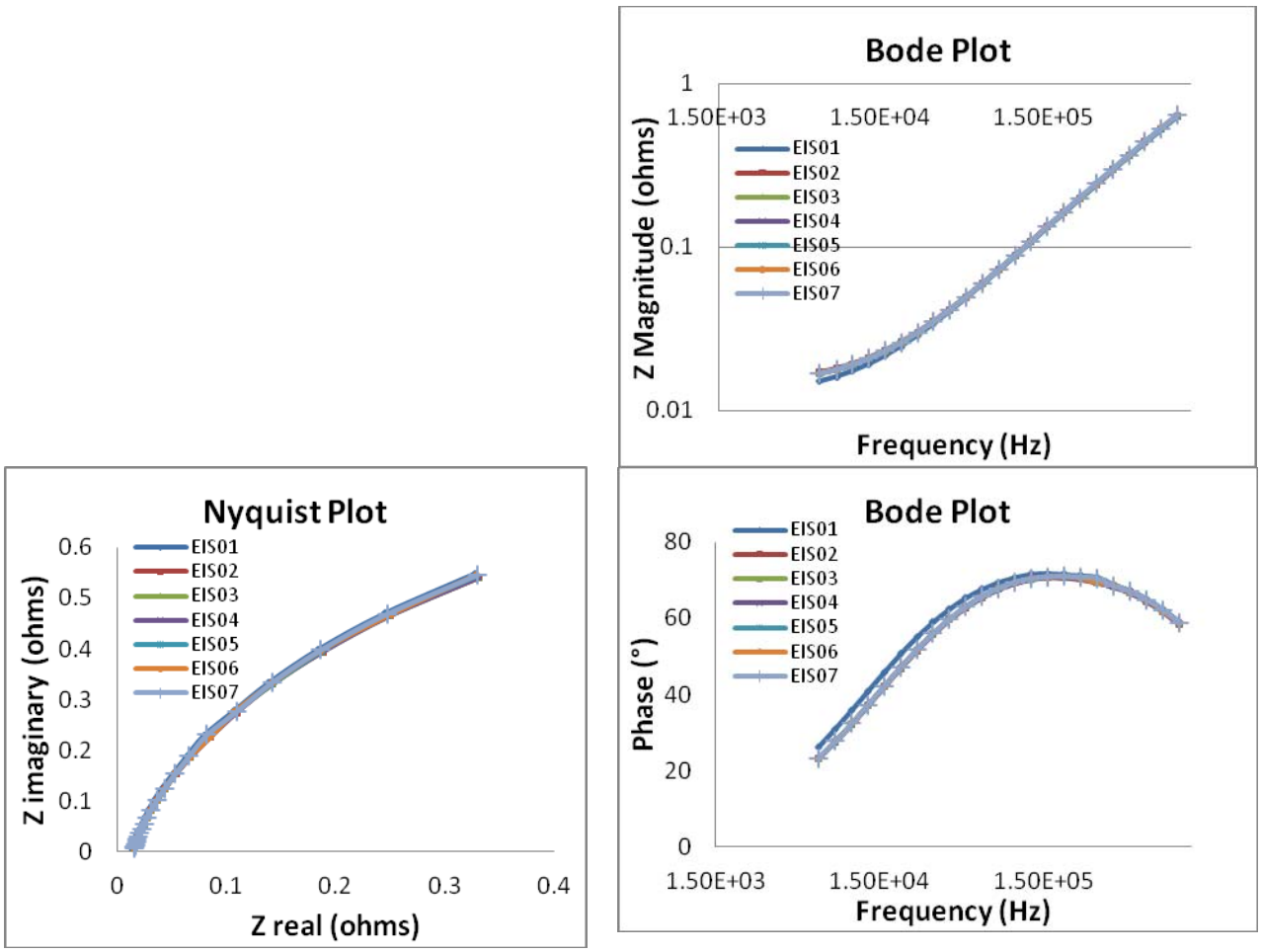

Figure 4.6: Nyquist and Bode plots for low pHe environment using static cylindrical 316L stainless steel in 60 volume % water, pHe = 3, 200°C, 0 ppm Cl^-.

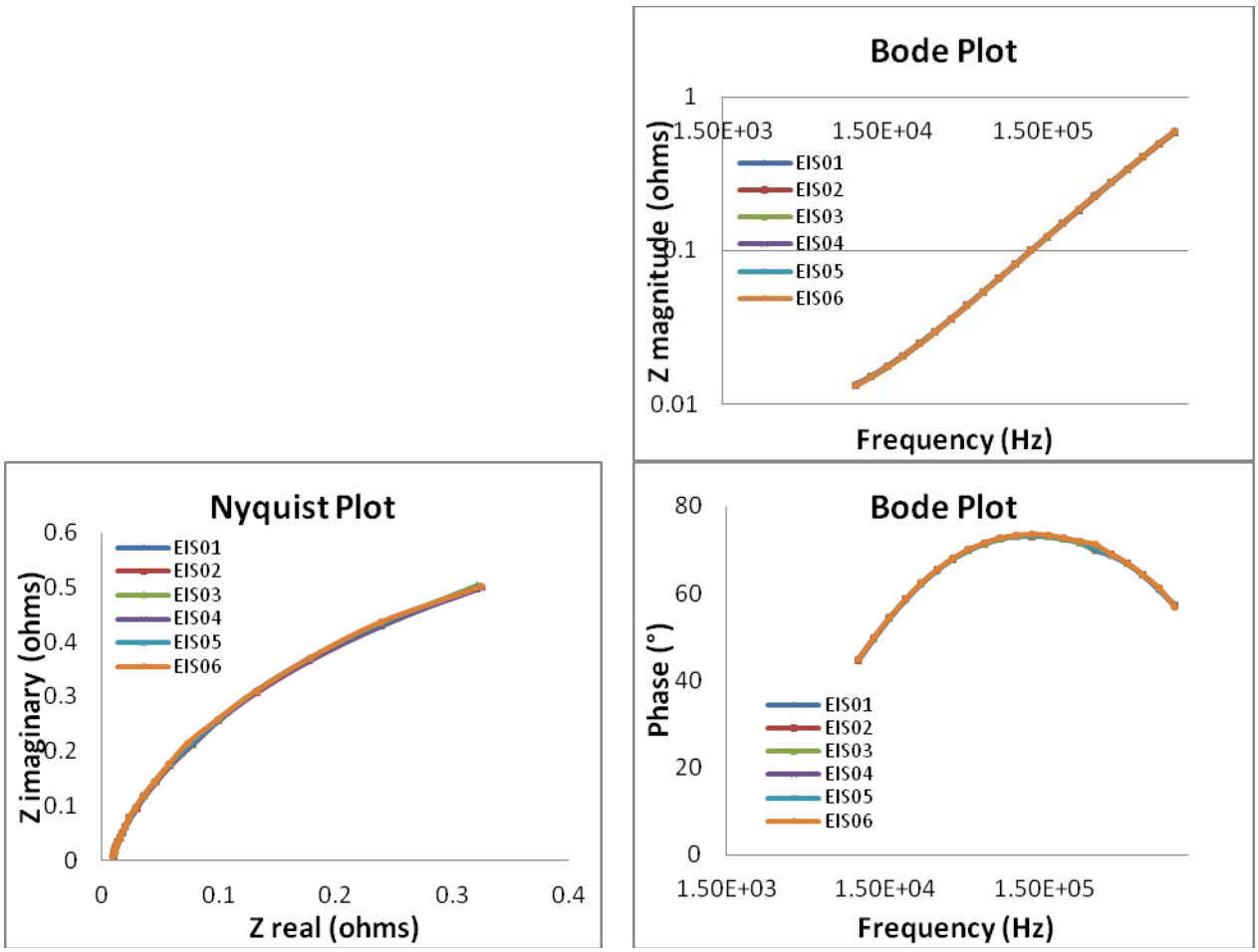

Figure 4.7: Nyquist and Bode plots for high Cl^- environment using static cylindrical 316L stainless steel in 60 volume % water, pHe = 6, 200°C, 50 ppm Cl^-.

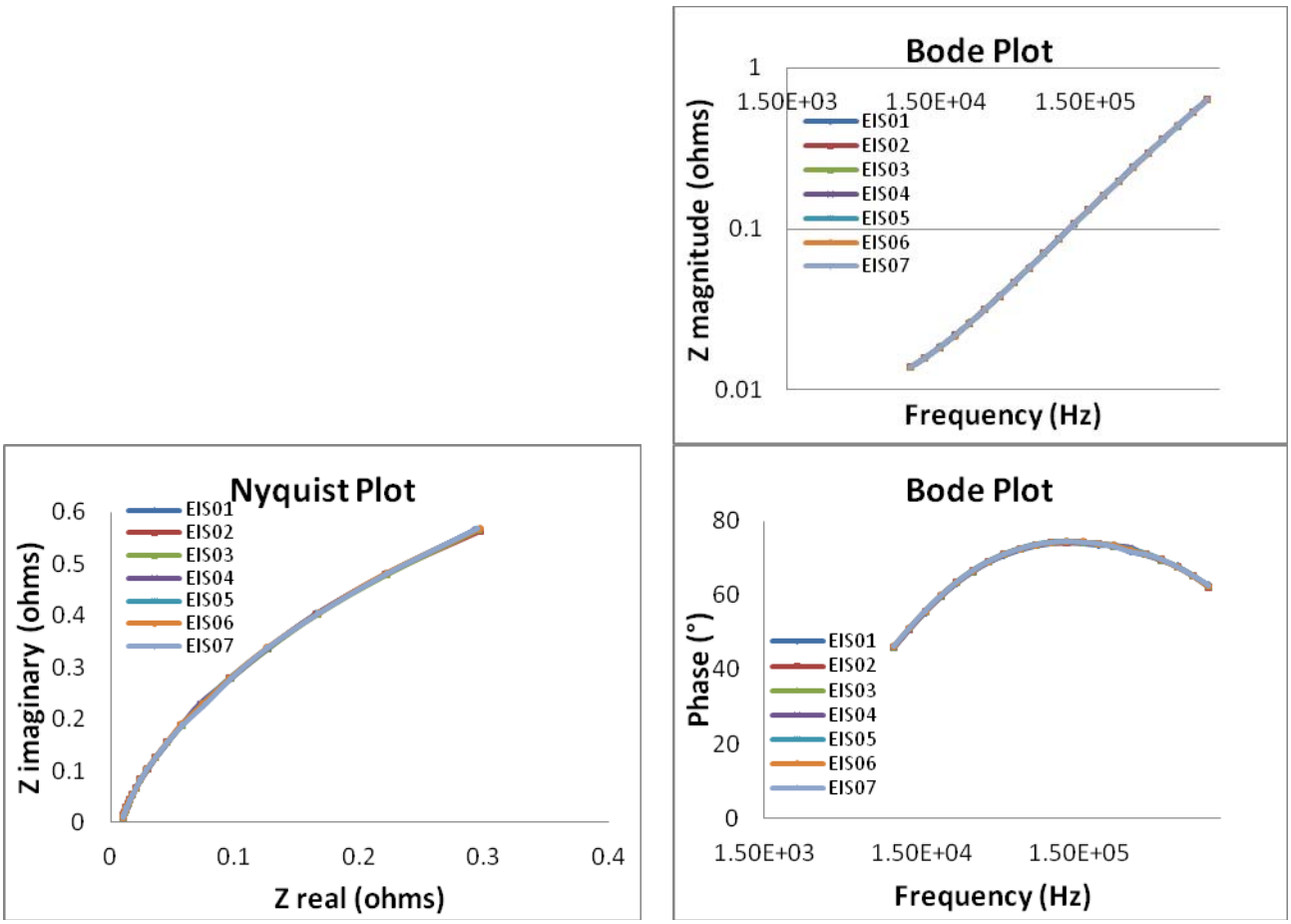

Figure 4.8: Nyquist and Bode plots for low pHe, high Cl^- environment using static cylindrical 316L stainless steel in 60 volume % water, pHe = 3, 200°C, 50 ppm Cl^-.

The data presented in Figure 4.9 compares the three test environments to each other via EIS data. In all three plots the low pHe and high Cl^- data appears to have the highest resistance, and the high Cl^- data has the lowest resistance when assuming the solution would be modeled as a simple circuit with a resistor (of the solution) in series with a capacitor (from the double layer) and resistor (for passivation) in parallel. There is significant overlap for all three environments though, so the pHe and Cl^- do not directly impact solution behavior. Rather since the water content and temperature are the same it is expected that those most impact film behavior.

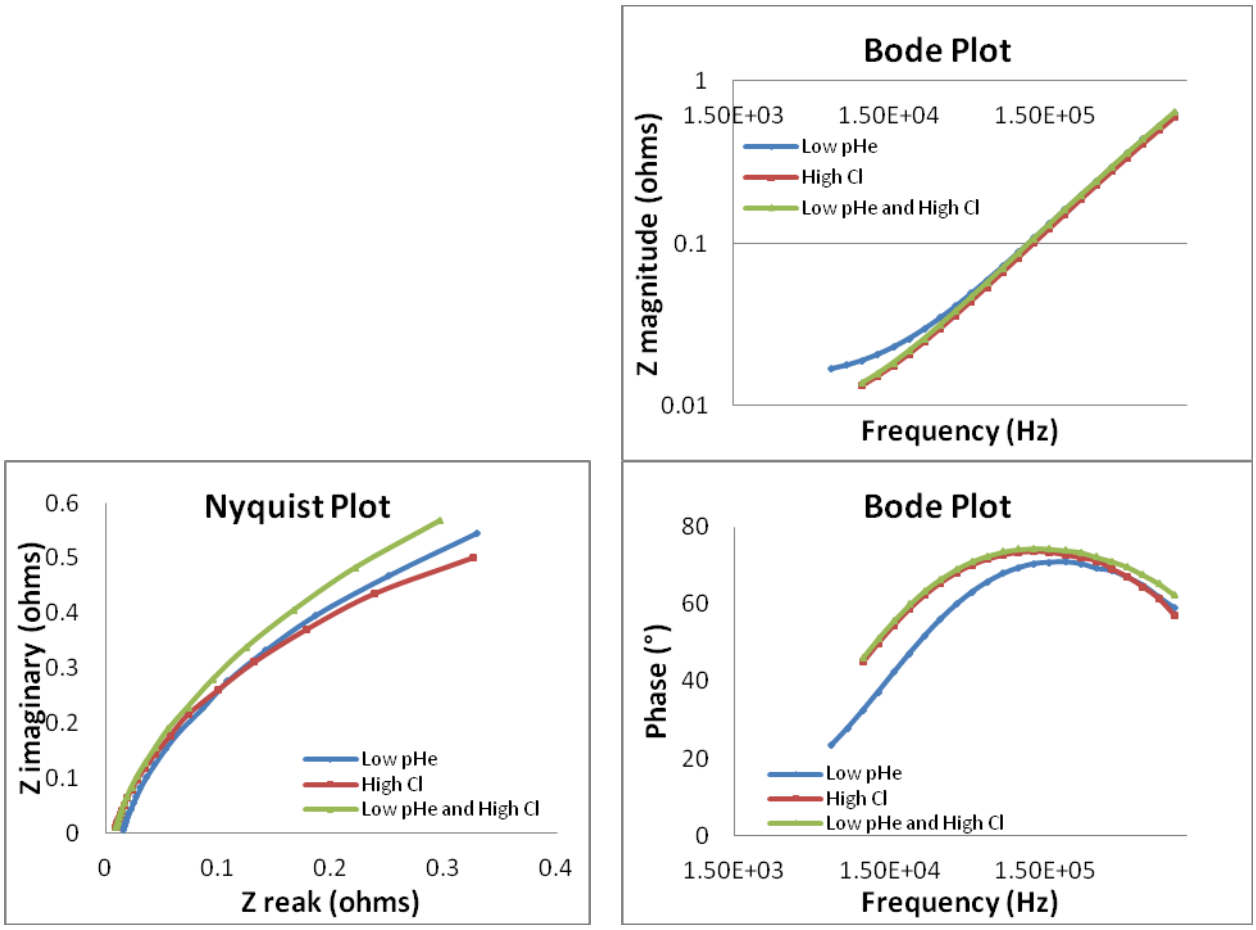

Figure 4.9: Nyquist and Bode comparison plots for the last electrochemical impedance spectroscopy tests of the low pHe, high Cl^-, and low pHe and high Cl^- test environments.

The electrochemical data further supports the corrosion data in that static samples show stable passive film on the 316L stainless steel surface. This also supports that the film needs to be disrupted, either by stress or through pitting, but crack formation and growth only occur with an added tensile stress. Both environments tested containing Cl^- showed evidence of pit initiation, with significantly more pits in the low pHe environment. This supports section 2.7.2 in the background, which concluded that acid can destabilize the film. Because more pits are present, it is likely that the film was less stable and more Cl^- were able to get to the sample surface to initiate pits in the low pHe, high Cl^- environment.

4.3 Localized Corrosion of 316L Stainless Steel in Ethanol/Water Environments

Evidence of localized corrosion was looked for in the immersion test sample and microstructural analysis was performed to understand the possible initiation sites. On most of the samples no surface film was visible and general corrosion did not occur. However, the samples listed in Table 4.3 did experience localized corrosion in the form of pitting.

Table 4.3: Immersion test samples that experienced pitting. Pit severity is compared by pits per area for immersion samples and pit density for tensile samples, looking at pits along the sides of the mounted cross sections.

Water (volume %)	Temperature (°C)	pHe	Cl- (ppm)	Corrosion Rate (mpy)	Pits per Area, Immersion Samples (pits/cm^2)	Pit Density, Tensile Samples (pits/cm)
60	200	6	5	0.043	0.6	0
60	175	6	50	0.286	1.3	0.13
60	200	6	10	0.360	2.2	0.04
60	200	6	30	1.088	3.2	0.31

All of the samples that showed pitting were in Cl^- containing environments and the pHe was 6. Unlike in the static electrochemical tests, pitting was not observed in solutions with lower pHe and 60 volume % water. Pitting only occurred in tests done at 175 or 200°C. This indicates that both water content and pHe may impact when pitting will occur in the system, once Cl^- is added. Data in Table 4.3 shows that the test at 175°C and 50 ppm Cl^- showed a lower pit density when compared to the 200°C, 30 ppm Cl^- sample. Although it is difficult to deduce the effect of temperature and Cl^- content from these results, the data showed that temperature impacts pitting susceptibility, with higher temperature promoting more pits on the sample surface.

The morphology of the pits can be seen in Figure 4.10. The 5 ppm Cl^- and 50 ppm Cl^-samples showed individual pits forming on the sample surface. On the other hand, the

10 ppm Cl^- and 30 ppm Cl^- samples showed long, worm-like strings of pits, as if small circular pits initiated near each other and grew to connect together. This data further supports that increasing temperature, more so than increasing Cl^- concentration, will increase pit severity. The 50 ppm Cl^- sample pit is approximately twice as large at the 5 ppm Cl^- sample, indicating that more Cl^- at a lower temperature is more severe than significantly fewer Cl^- at a higher temperature. At the same temperature however, the 30 ppm Cl^- sample shows a much longer, thicker pit.

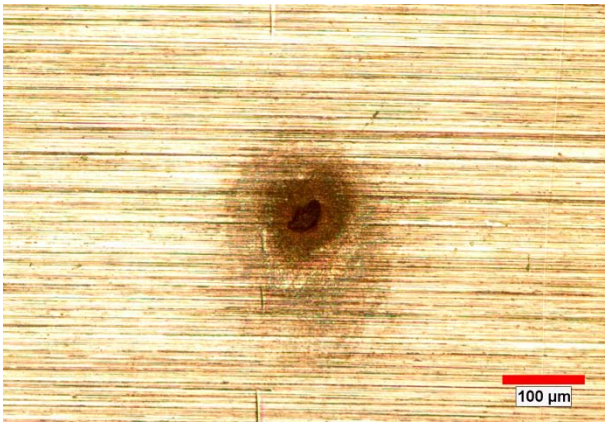

5 ppm Cl-, 200°C, With Film

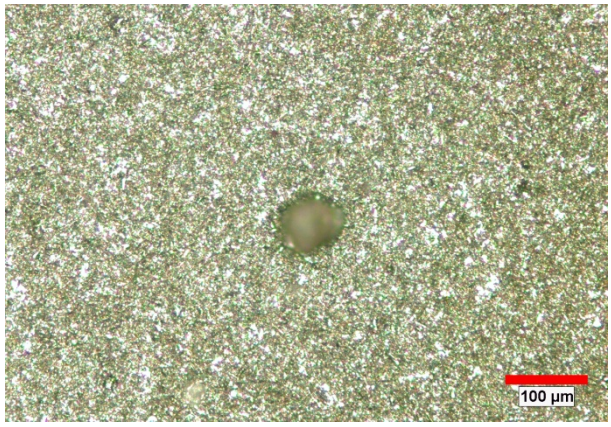

50 ppm Cl-, 175°C, Film Removed

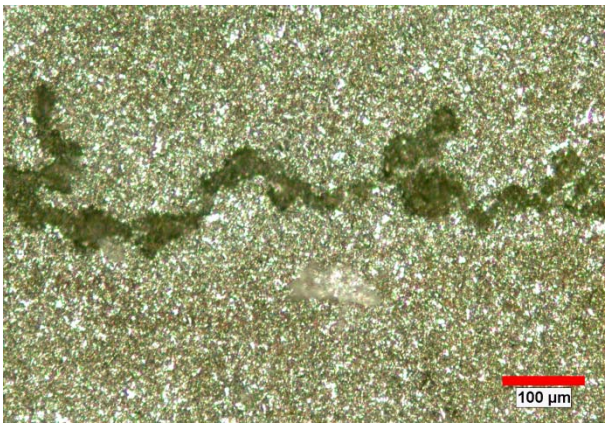

10 ppm Cl-, 200°C, Film Removed

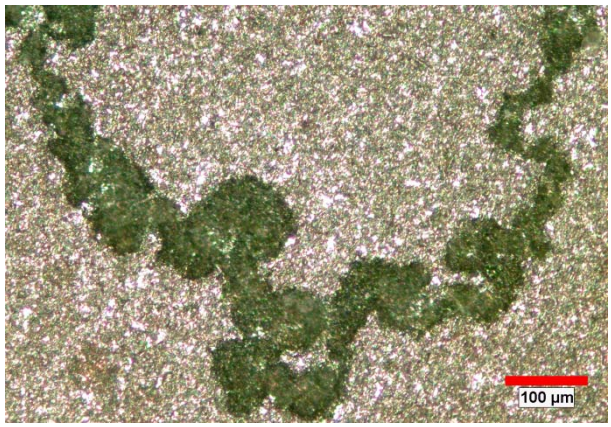

30 ppm Cl-, 200°C, Film Removed

Figure 4.10: Pit morphology for the four immersion samples listed in Table 4.3. All samples were in a 60 volume % water, pHe = 6 environment. In the top left image with the film still intact, polish lines do not run through the pit and it is recessed. The other three images have the film removed and show indentations of pits remaining in the sample surface. Because the pits are recessed from the surface they are not in focus.

Cl^- contamination is a serious concern for organsolv delignification environments, especially at the higher end of the temperature range. Table 4.3 and Figure 4.6 indicate that concentrations at small as 10 ppm Cl^- can initiate pits, and that a three-fold increase in this concentration leads to nearly a three-fold increase in pit density, with connected, worm-like pits that are approximately three times thicker and at least twice as long.

4.4 Microstructural Analysis of 316L Stainless Steel

To understand where the pits could initiate on the 316L stainless steel surface, microstructural analysis was performed on the immersion test samples and slow strain rate specimens to compare the microstructural features of the two types of samples.

Grain size was compared between the two to determine if one set of samples contained more grain boundaries, a possible crack initiation site, than the other. The results are presented in Tables 4.4 and 4.5, which show that all samples and directions have comparable ASTM grain size numbers around 7. Based on the published literature for stainless steels in Cl^- containing environments, the grain boundaries only act as crack initiation sites if they contain chromium carbide precipitates from sensitization. These precipitates increase corrosion susceptibility around grain boundaries by pulling Cr, a corrosion resistant alloying element, from the surrounding matrix. The microstructure of tested 316L stainless steel was analyzed for the presence of these precipitates. As expected, Figure 4.11 shows no evidence of chromium carbide precipitates along the grain boundaries of the 316L stainless steel.

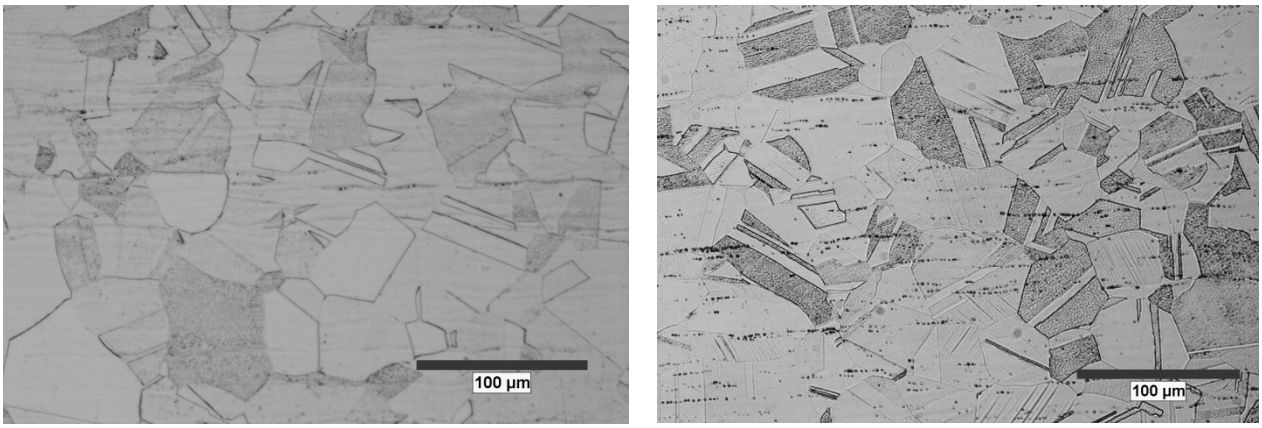

Immersion Sample Tensile Sample

Figure 4.11: Representative microstructures of the immersion test samples (left) and tensile test samples (right) both showing stringers running parallel to the top and bottom edges of the images.

Table 4.4: Grain size calculated for five slow strain rate test samples.

Sample	Longitudinal Perpendicular to Stringers	Longitudinal Parallel to Stringers	Transverse Short Edge	Transverse Long Edge
SSRTb	7.7 +/- 3.0	7.3 +/- 1.7	7.3 +/- 3.1	7.0 +/- 2.5
SSRTe	7.2 +/- 2.7	6.6 +/- 1.4	7.1 +/- 2.9	7.0 +/- 2.2
SSRTm	7.2 +/- 2.8	6.7 +/- 2.0	7.1 +/- 3.4	6.8 +/- 2.5
SSRTq3	6.9 +/- 2.5	6.7 +/- 2.8	7.5 +/- 2.8	7.2 +/- 2.6
SSRT2	7.5 +/- 3.4	6.8 +/- 1.9	7.6 +/- 1.7	7.5 +/- 1.5

Table 4.5: Grain size calculated for one immersion test sample. All immersion samples came from the same stock.

Sample	Side 1 Long	Side 1 Short	Side 2 Long	Side 2 Short	Side 3 Long	Side 3 Short
Immersion	6.7 +/- 2.0	6.7 +/- 2.6	6.8 +/- 2.2	6.8 +/- 2.2	6.9 +/- 1.9	6.5 +/- 2.3

The etched microstructures of the samples indicated the presence of inclusions in the form of stringers, shown in Figure 4.11. The volume fraction of the stringers is reported in Table 4.6, where the tensile samples have more stringers per unit volume. Also, the severity of the stringers is worse as seen in the stringer characterization in Table 4.7. The stringers in the tensile samples are larger and contain significantly more in a given field of view. This data is supported by the images in Figure 4.11, where the immersion sample has significantly fewer stringers than the tensile test sample. Based on

earlier research suggesting Cl^- induces pitting in stainless steels preferentially at MnS inclusions, it is suspected the stringers are MnS based and are the initiation sites for pits in both immersion and tensile samples.

Table 4.6: Volume fraction of inclusions in slow strain rate test samples and the immersion test sample.

Sample	Longitudinal (Side 1)	Transverse (Side 2)	Side 3
SSRTb	0.052 +/- 0.047	0.063 +/- 0.079	----------
SSRTe	0.052 +/- 0.047	0.063 +/- 0.056	----------
SSRTm	0.042 +/- 0.076	0.073 +/- 0.076	----------
SSRTq3	0.104 +/- 0.065	0.052 +/- 0.026	----------
SSRT2	0.052 +/- 0.047	0.031 +/- 0.034	----------
Immersion	0.010 +/- 0.026	0.010 +/- 0.026	0.021 +/- 0.032

Table 4.7: Inclusion characterization of the microstructures studied. The first number indicates the longest stringer found in the field of view. T denotes it was thin (<10 um thick) and vd means it was very disconnected. The second number indicates the average length of the other stringers found in that field of view, and the superscript of that number shows how many stringers were averaged to get that number.

Sample	#1	#2	#3	#4	#5	#6
SSRTb	$1^{T}_{vd}\text{-}1^{7}$	$2^{T}_{vd}\text{-}1^{5}$	$3^{T}_{vd}\text{-}1^{5}$	$3^{T}_{vd}\text{-}1^{6}$	$2^{T}_{vd}\text{-}1^{6}$	$2^{T}_{vd}\text{-}1^{5}$
SSRTe	$1^{T}_{vd}\text{-}1^{4}$	$2^{T}_{vd}\text{-}1^{7}$	$3^{T}_{vd}\text{-}1^{10}$	$2^{T}_{vd}\text{-}1^{11}$	$1^{T}_{vd}\text{-}1^{3}$	$2^{T}_{vd}\text{-}1^{9}$
SSRTm	$2^{T}_{vd}\text{-}1^{9}$	$3^{T}_{vd}\text{-}1^{6}$	$2^{T}_{vd}\text{-}1^{8}$	$2^{T}_{vd}\text{-}1^{6}$	$2^{T}_{vd}\text{-}1^{7}$	$3^{T}_{vd}\text{-}1^{8}$
SSRTq3	$2^{T}_{vd}\text{-}1^{5}$	$2^{T}_{vd}\text{-}1^{3}$	$1^{T}_{vd}\text{-}1^{3}$	$2^{T}_{vd}\text{-}1^{4}$	$2^{T}_{vd}\text{-}1^{6}$	$2^{T}_{vd}\text{-}1^{5}$
SSRT2	$3^{T}_{vd}\text{-}1^{8}$	$2^{T}_{vd}\text{-}1^{7}$	$2^{T}_{vd}\text{-}1^{8}$	$2^{T}_{vd}\text{-}1^{11}$	$2^{T}_{vd}\text{-}1^{8}$	$2^{T}_{vd}\text{-}1^{10}$
Immersion	$1^{T}_{vd}\text{-}0^{0}$	$2^{T}_{vd}\text{-}1^{2}$	$1^{T}_{vd}\text{-}1^{1}$	$2^{T}_{vd}\text{-}1^{1}$	$1^{T}_{vd}\text{-}1^{1}$	0

Only two possible microstructure-influenced crack initiation sites were seen: grain boundaries and inclusions. There was no evidence of secondary phases in the microstructure. Of these, it seems more probable that the inclusions are initiation sites because there was no visual evidence of composition variation along the grain boundaries. As the pits grow from circle to worm-like, it is plausible their shape is dependent on the feature they initiated from. While the stringers are mostly straight, they do have some curvature, which could account for the worm-like pattern seen in high Cl^- containing samples.

4.5 Pit Initiation Sites on 316L Stainless Steel Surface

SEM with EDX data was taken to analyze how the stringers in the microstructure impacted pit initiations for the immersion test samples that experienced pitting. Figures 4.12-4.14 show compositional data for the worst case scenario of 30 ppm Cl^- at 200°C. Figures 4.12 and 4.13 showed compositional analysis of the pits with and without the passive film, respectively. As expected for austenitic stainless steels, the passive film on top of the pitted area consists primarily of Cr and O, suggesting it could be the Cr_2O_3 film known to passivate 316L. The data indicated 0.15 weight % S and 0.03 weight % Mn exist here, suggesting this area is nearly devoid of Mn and rich in S. When the film is removed from the pit and compositional data is taken, as in Figure 4.13, similar weight %s of S and Mn are seen at 0.08 and 0.17 respectively. These values do not fall within the nominal compositions of S and Mn seen in Table 3.1. Further, an EDX spectra for a non-pitted area of the sample showed 0.15 weight % S and 1.09 weight % Mn.

This data indicates that the sulfur content is read as high throughout the surface of the metal. The values indicate 3 to 5 times more S than the nominal composition for 316L. The discrepancies in these values can be explained as poor calibration of the EDX instrument or S contamination in the stainless steel. However, relatively speaking more S and Mn are seen in the base metal than at the pits, possibly indicating that Mn and S that had been present around the pits dissolved. Pits typically form at MnS inclusions (Section 2.2), and when they form they dissolve the MnS inclusions and react with the base metal. This would explain the lack of MnS in the pits because the inclusions are already dissolved and the base metal has reacted to form an excess of a chromium oxide film on the pit, as seen in Figure 4.12.

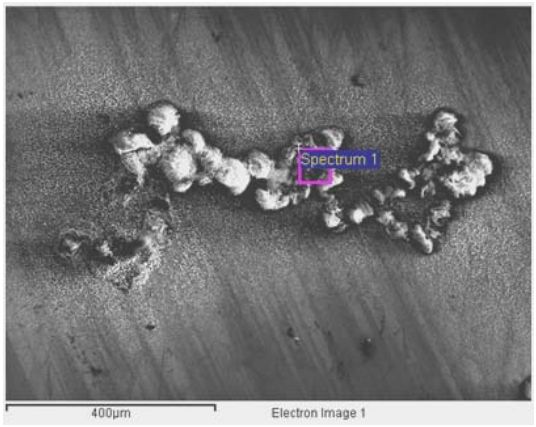

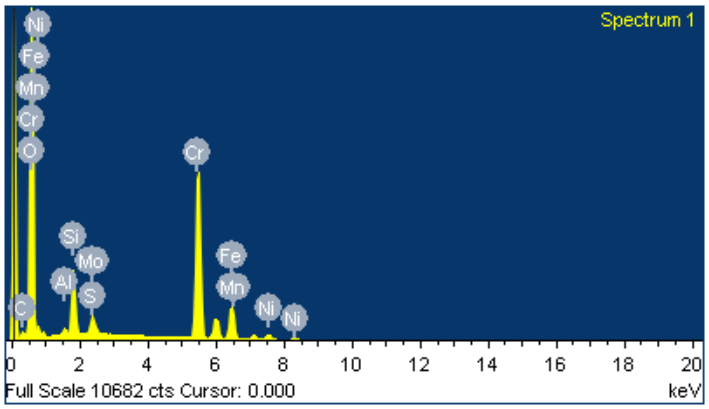

Figure 4.12: SEM image (left) and EDX spectra (right) of a pit in 60 volume % water, 200°C, pHe = 6, 30 ppm Cl^- environment without removal of the passive film. The bulbous deposit above the pit is corrosion product.

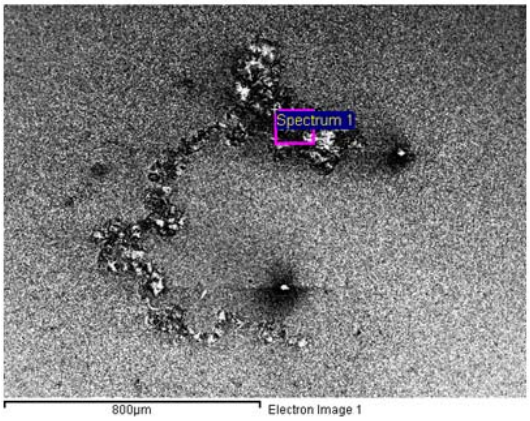

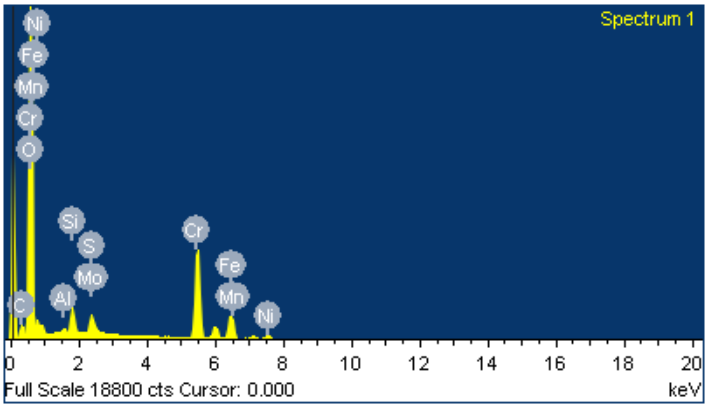

Figure 4.13: SEM image (left) and EDX spectra (right) of a pit in 60 volume % water, 200°C, pHe = 6, 30 ppm Cl^- environment with the passive film removed. The pit was still visible as an indentation in the sample surface.

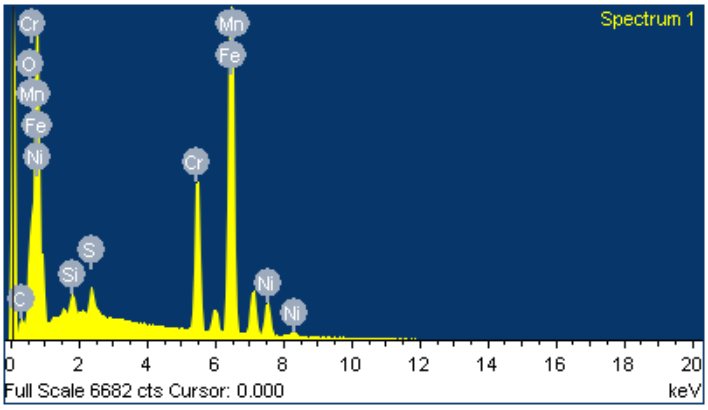

Figure 4.14: EDX spectra of base metal in 60 volume % water, 200°C, pHe = 6, 30 ppm Cl^- environment without removal of the passive film. The spot was away from any pits on the sample surface.

The results for the 50 ppm Cl^-, 175°C sample are presented in Figures 4.15 and 4.16. Like the 30 ppm Cl-, 200°C sample, this sample shows a Cr and O based film covering the pit. It shows significantly more S at 1.82 weight % and slightly more Mn at 0.19 weight %. The base metal shows less S at 0.12 weight % and more Mn at 1.19 weight %. The base metal S and Mn contents for this sample are comparable to those in Figure 4.14. As before, there is less Mn in the pit than in the base metal, suggesting that the Mn in the inclusion has dissolved. However, more S is seen near the pit. This suggests that S is still in excess in the area and has yet to dissolve indicating the pit was sulfur based. S can poison repassivation of a pit once it has initiation (Section 2.2), which is why it may be more prevalent at this pit because it has yet to dissolve.

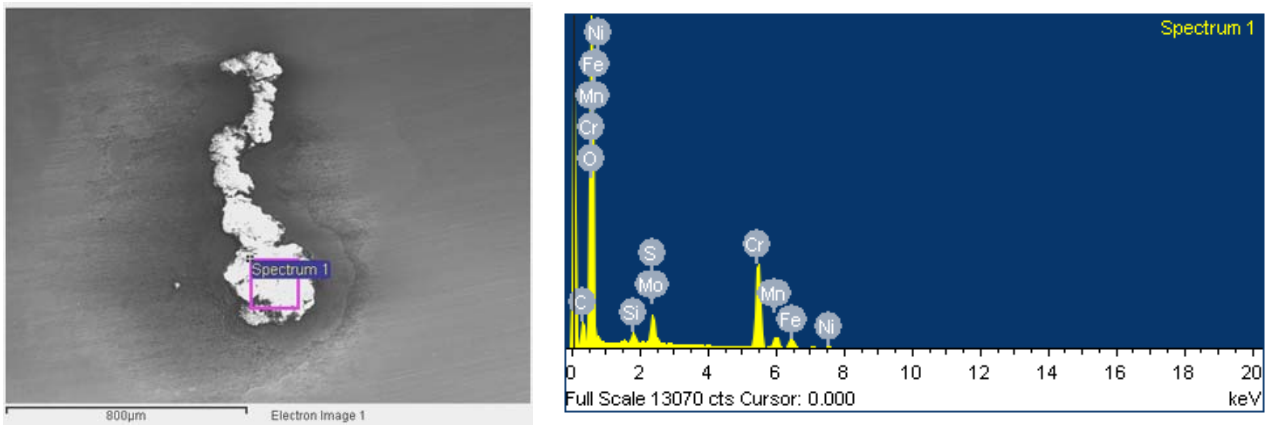

Figure 4.15: *SEM image (left) and EDX spectra (right) of a pit in 60 volume % water, 175°C, pHe = 6, 50 ppm Cl^- environment without removal of the passive film. The bulbous deposit above the pit is corrosion product.*

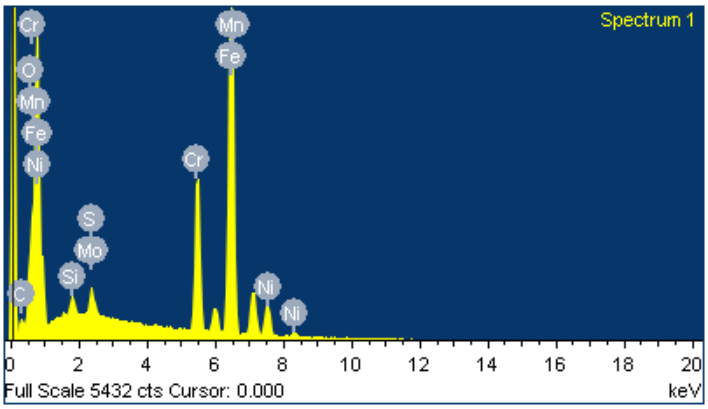

Figure 4.16: *EDX spectra of base metal in 60 volume % water, 175°C, pHe = 6, 50 ppm Cl^- environment without removal of the passive film. The spot was away from any pits on the sample surface.*

The SEM and EDX analysis for the pitted immersion samples indicate the pits are likely initiating at MnS inclusions. However, most of the pits have already dissolved the inclusion and are coated in a passive chromium oxide layer from the base metal reacting with the solution. The cleaner the steel, and the fewer inclusions that it contains, then the less likely pits will form on the surface.

4.6 Conclusions

The data indicated that in acidic ethanol/water environments the passive film that forms on the sample surface is stable under static conditions. It protects the bulk of the metal from corrosion and no surface activity was evident. However, in Cl^- containing ethanol/water environments localized corrosion in the form of pitting is induced by Cl^- ions. These pits, which are likely initiating at MnS inclusions, readily grow, especially with increased temperature. In Cl^- containing environments, it is likely the pits can initiate cracking.

This data indicates that it is particularly important to pay attention to temperature and Cl^- content of organosolv delignification environments. An increase in temperature from 175°C to 200°C showed significant increase in the severity of pitting, even with decreasing Cl^- concentration (50 ppm vs. 30 ppm, respectively). At 200°C even 10 ppm Cl^- showed significant pitting, which could lead to rapid industrial failures. Ideally, the Cl^- contamination from the biomass or process stream would be minimized to prevent Cl^- induced SCC.

CHAPTER 5

STRESS CORROSION CRACKING BEHAVIOR OF 316L AUSTENITIC STAINLESS STEEL

Initial SCC susceptibility of 316L stainless steel was tested for a wide range of environments related to the organosolv delignification environments in Table 2.1. The tests ranged from 0 - 100 volume% water, 100 - 220°C, pHe between 2 - 8, and 0 - 100 ppm Cl^-. General trends in the corrosion and stress corrosion cracking susceptibility of 316L stainless steel were seen in this data, including the threshold value of each environmental variable. From there, tests were done to understand how changing each variable impacted SCC, followed by a focused study to understand the impact of changing water and temperature for a fixed pHe and Cl^- content.

5.1 General Trends of SCC of 316L Stainless Steel in Ethanol/Water Environments

Initial tests were carried out in solutions with a broad range of parameters. Of the four variables tested, water content and temperature of the solution most affected the SCC susceptibility of 316L in ethanol/water environments. As can be seen in Figure 5.1, no SCC occurred at water contents of 0 and 1 volume %, however with 10 volume % water some environments showed SCC susceptibility. SCC was also seen in environments with significant water contents, including up to 90 volume %. This suggests that there is a minimum value of water needed for cracking to occur. This may be because the water affects the passivation behavior of the stainless steel surface. In order to allow a stable film to form on the sample surface, which is necessary for SCC, the data suggests that the water content needs to be at least 10 volume %.

Figure 5.1 also shows the significant impact of temperature on SCC susceptibility. Depending on the environment, there exists a temperature threshold between 150 and 200°C below which SCC does not occur. However, this value is also dependent on the other environmental parameters. Environments containing Cl^- with no added acid can induce SCC at 175°C, while environments with acid and no Cl^- only showed cracking at 200°C.

In order for SCC of 316L stainless steel to occur, the environment needs to be at or above the minimum values for water content and temperature. The other two variables, pHe and Cl^-, play a secondary role and only one of these threshold conditions needs to be met for SCC. This data is supported by the information presented in Figure 5.1. Of the four combinations of pHe and Cl^- conditions, when the environment was above the pHe and below the Cl^- thresholds (the red squares) SCC of 316L stainless steel was not detected. In the other three conditions in which either one or both pHe was below and Cl^- was above the threshold value, SCC of 316L stainless steel was observed.

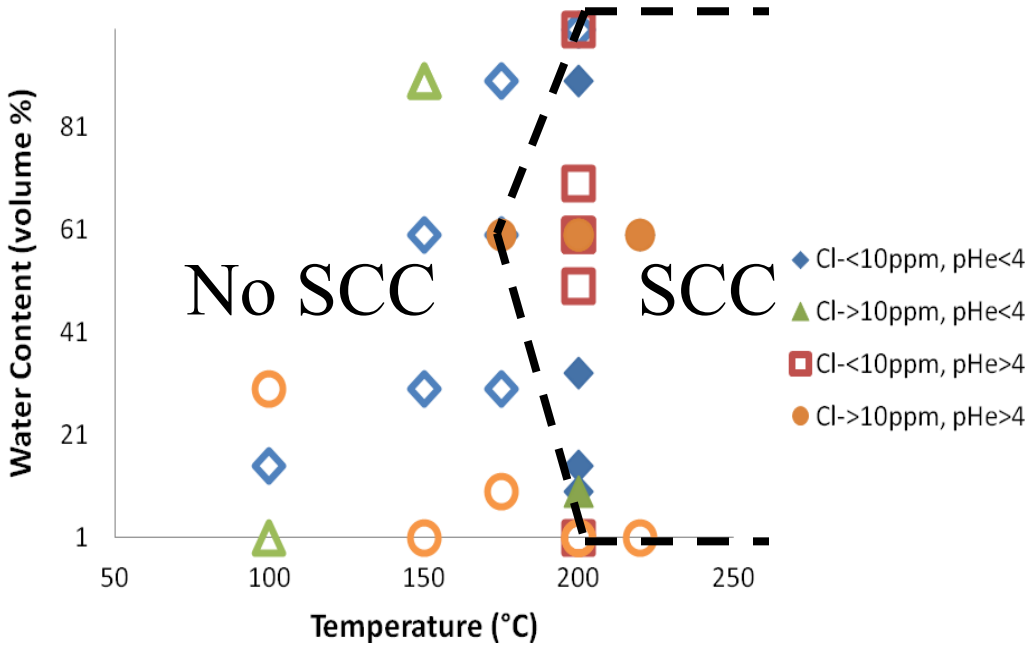

Figure 5.1: Overall trends for water and temperature effects on stress corrosion cracking of high temperature ethanol/water environments. Open data points indicate stress corrosion cracking did not occur and closed data points indicate stress corrosion cracking occurred. The pHe and Cl^- data is presented for experiments as being above or below the threshold values.

The threshold values for pHe and Cl^- concentration were tested for ethanol/water solutions with 60 volume % water, at 200°C. When pHe effect was being tested, no Cl^- was added to the environment, similarly when Cl^- was being studied, pHe was not adjusted. The pHe threshold was found to be around 4 and the Cl^- threshold around 10 ppm, as can be seen in Figure 5.2. SCC only occurred when the conditions were above both the water and temperature thresholds, and once within the water threshold (i.e. greater than 1 volume% water and less than 100 volume %), but below the temperature threshold at 175°C. This environment did contain 50 ppm Cl^-. The remaining two test conditions, below water threshold and above threshold temperature, with both water content and temperature below the threshold did not show any instances of SCC. This data supports that under most environmental conditions, the water and temperature both

need to be above the threshold values for SCC to occur in these systems. It is suspected that Cl^- may shift these thresholds, as evidenced by the only test where SCC was observed at 175°C.

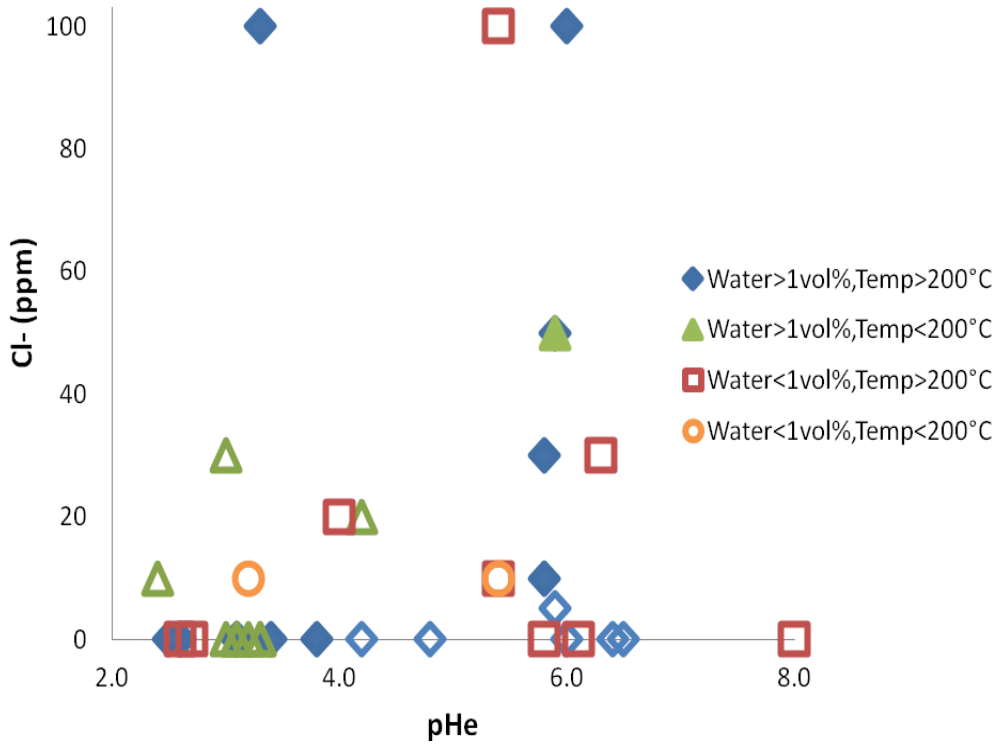

Figure 5.2 Overall trends for pHe and Cl^- effects on stress corrosion cracking of high temperature ethanol/water environments. Open data points indicate stress corrosion cracking did not occur and closed data points indicate stress corrosion cracking occurred. The water and temperature data is presented for experiments as being above or below the threshold values.

Figures 5.4-5.6 show crack shape and morphology for variable pHe, fixed Cl^- environments and Figure 5.7 shows crack morphology for fixed pHe, variable Cl^- environments. When the Cl^- concentration was fixed but the pHe was varied, the cracks were carrot shaped and found throughout the gage length, though they were concentrated near the fracture surface. When pHe was fixed, the cracks were found to be associated with pits. The cracks were either near pits or inside of them, and were skinny and

branched. Only one 316L sample tested at 10 volume% water and 200°C failed by SCC when the chloride content was above the threshold and the pHe of the solution was below the threshold value (i.e. pHe = 3, 100 ppm Cl-). The cracks in this sample, seen in Figure 5.3, resemble the carrot shaped cracks in Figures 5.4-5.6, indicating the crack mode is similar to what was seen in fixed Cl^- environments.

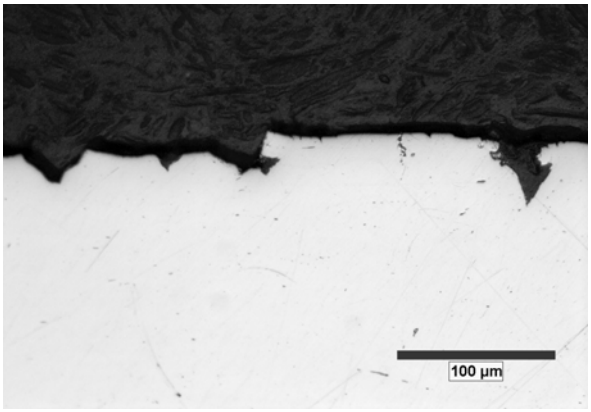

Figure 5.3: Cross section of the only sample tested above temperature, water, and Cl^- thresholds and below pHe threshold. The sample was in a 10 volume % water, 100 ppm Cl^-, pHe =3, 200°C environment.

5.2 Effect of Environmental Variables on Stress Corrosion Cracking Susceptibility of 316L Stainless Steel

Once the general trends were understood, each variable was varied to study its impact on SCC severity. For this, the standard environment used was 60 volume % water, 200°C, 0 ppm Cl^-, and pHe = 3, which is comparable to the organsolv delignification environments in Table 2.1.

The environment used to test water effects are listed in Table 5.1 where all other parameters were kept constant except for the water content, which increased from 15 volume % to 60 volume %. Results in Table 5.1 and Figure 5.5 indicate that the crack density was not impacted by increasing water content. However, the crack velocity more

than doubled with the quadrupling of the water content (and simultaneous quartering of the ethanol content), as shown in Table 5.1. Water content seems to affect crack growth rate, but not crack density. Cracks grow faster with increasing water content. Figure 5.5 indicates that 316L samples tested in solutions with different water content showed wide carrot-shaped cracks on the sample surface, with pointed crack tips propagating into the sample, similar to the crack morphology found for the samples tested in fixed Cl^- environments.

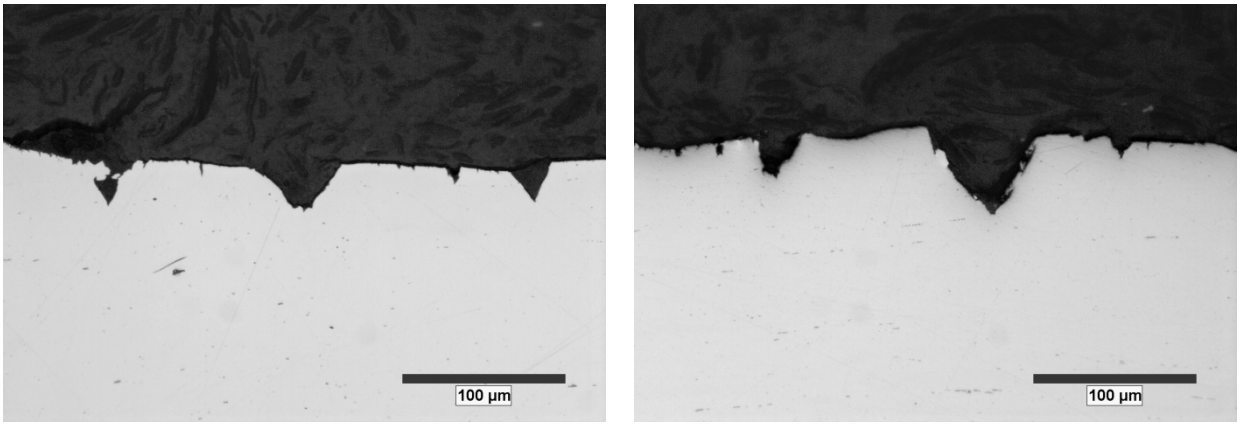

Low Water (15 vol %) High Water (60 vol %)

Figure 5.4: Impact of water content on 316L tensile samples showing cross sections of the deepest cracks found along the sample surface. The test environments are detailed in Table 5.1.

Table 5.1: Environments and resulting crack density and velocity for 316L tensile samples evaluating water content impact on stress corrosion cracking severity.

Sample	Water (vol%)	Cl- (ppm)	pHe	Temperature (°C)	Crack Density (cracks/mm)	Crack Velocity (mm/s)
Low Water	15	0	2.6	200	26 +/- 11	1.54E-7
High Water	60	0	2.4	200	33 +/- 11	3.30E-7

Table 5.2 shows the environment used to study effect of temperature on SCC. The crack densities for these two temperatures are comparable, indicating that temperature does not affect crack density on the sample surface. However, the cracks grow twice as

fast at 220°C than at 200°C, indicating that SCC severity increases with increasing temperature. Figure 5.5 shows representative cross sections of the samples, indicating carrot-shaped cracks with a much deeper and sharper crack at 220°C.

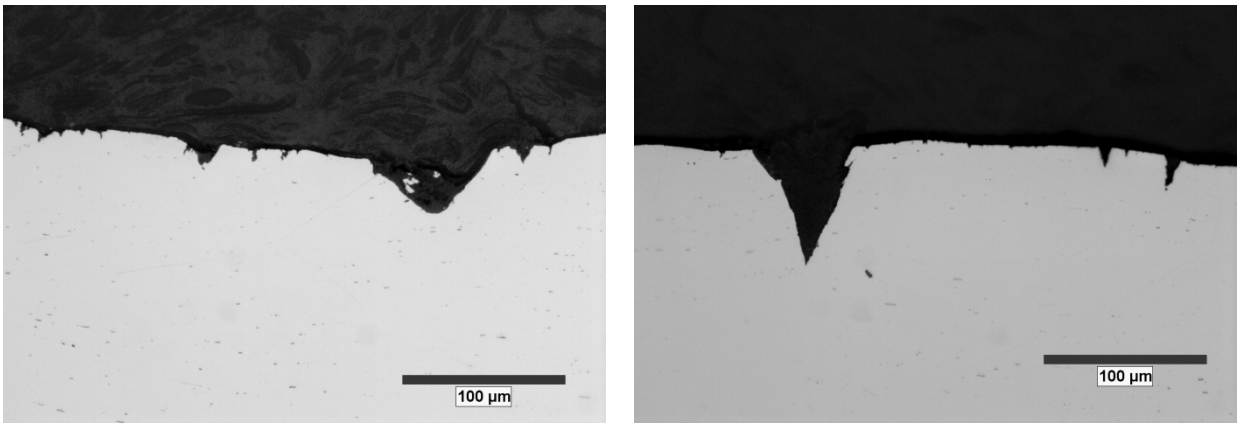

Low Temperature (200°C) High Temperature (220°C)

Figure 5.5: Impact of temperature on 316L tensile samples showing cross sections of the deepest cracks found along the sample surface. The test environments are detailed in Table 5.2.

Table 5.2: Environments and resulting crack density and velocity for 316L tensile samples evaluating temperature impact on stress corrosion cracking severity.

Sample	Water (vol%)	Cl- (ppm)	pHe	Temperature (°C)	Crack Density (cracks/mm)	Crack Velocity (mm/s)
Low Temperature	60	0	3.1	200	46 +/- 2	2.17E-7
High Temperature	60	0	3.1	220	50 +/- 11	4.28E-7

The effects of pHe can be seen in Table 5.3. Unlike water and temperature effects, decreasing the pHe, (i.e. increasing the acidity of the environment) caused fewer cracks to initiate on the sample surface. However, the cracks that do initiate propagate faster. This makes it difficult to determine which of the tested environments is more severe. In Figure 5.6, pHe = 3.1 shows more cracks on the sample surface than the pHe = 2.5. The crack density values are more comparable than the crack velocity, so lower pHe solutions

are more severe towards causing SCC of 316L in ethanol/water environments. As expected, these cracks are carrot shaped and found all along the sample gage.

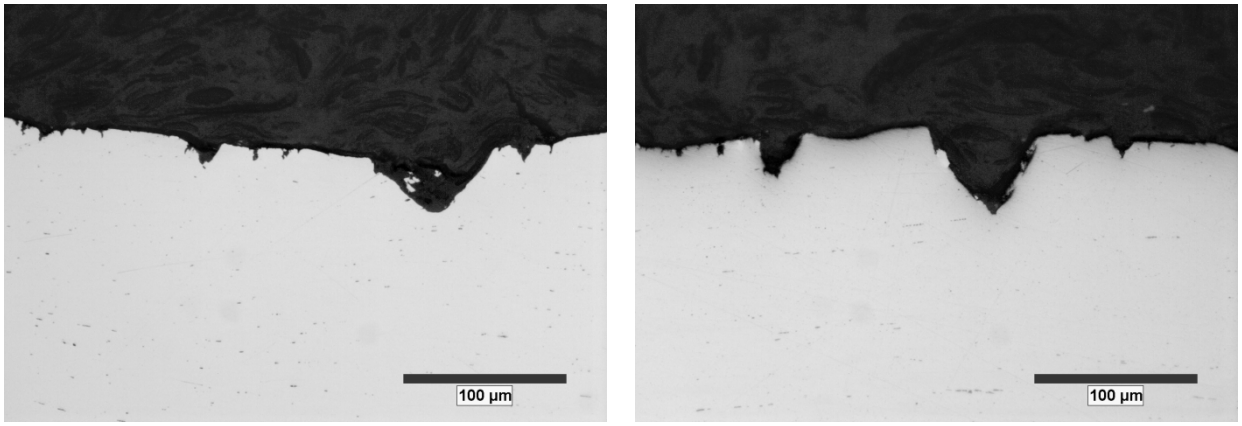

High pHe (3.1) Low pHe (2.5)

Figure 5.6: Impact of pHe on 316L tensile samples showing cross sections of the deepest cracks found along the sample surface. The test environments are detailed in Table 5.3.

Table 5.3: Environments and resulting crack density and velocity for 316L tensile samples evaluating pHe impact on stress corrosion cracking severity.

Sample	Water (vol%)	Cl- (ppm)	pHe	Temperature (°C)	Crack Density (cracks/mm)	Crack Velocity (mm/s)
High pHe	60	0	3.1	200	46 +/- 2	2.17E-7
Low pHe	60	0	2.5	200	33 +/- 11	3.30E-7

The environments used to test Cl^- effects are described in Table 5.4. Unlike the other environments where crack density was used as a comparison, pit density was used because all the cracks in the sample were associated with pits. When the Cl^- content was tripled, Table 4 indicates that the pit density increased nearly 8-fold. Varying Cl^- content was seen to have the most significant impact on SCC severity, with increasing Cl^- content increasing SCC severity. Not only were more pits present, but the cracks propagated over a magnitude faster when the Cl^- content was tripled from 10 to 30 ppm. These environments predominantly showed cracks associated with the initially formed pit, as can be seen in Figure 5.7. Both 10 ppm Cl^- and 30 ppm Cl^- showed pitting along the gage

of the tensile sample, but the pits were much larger in the 30 ppm Cl^- sample. A crack can be seen in the top right image of Figure 5.7 emanating from the pit, indicated by the red arrow. This further supports that cracks on the sample are only associated with pits.

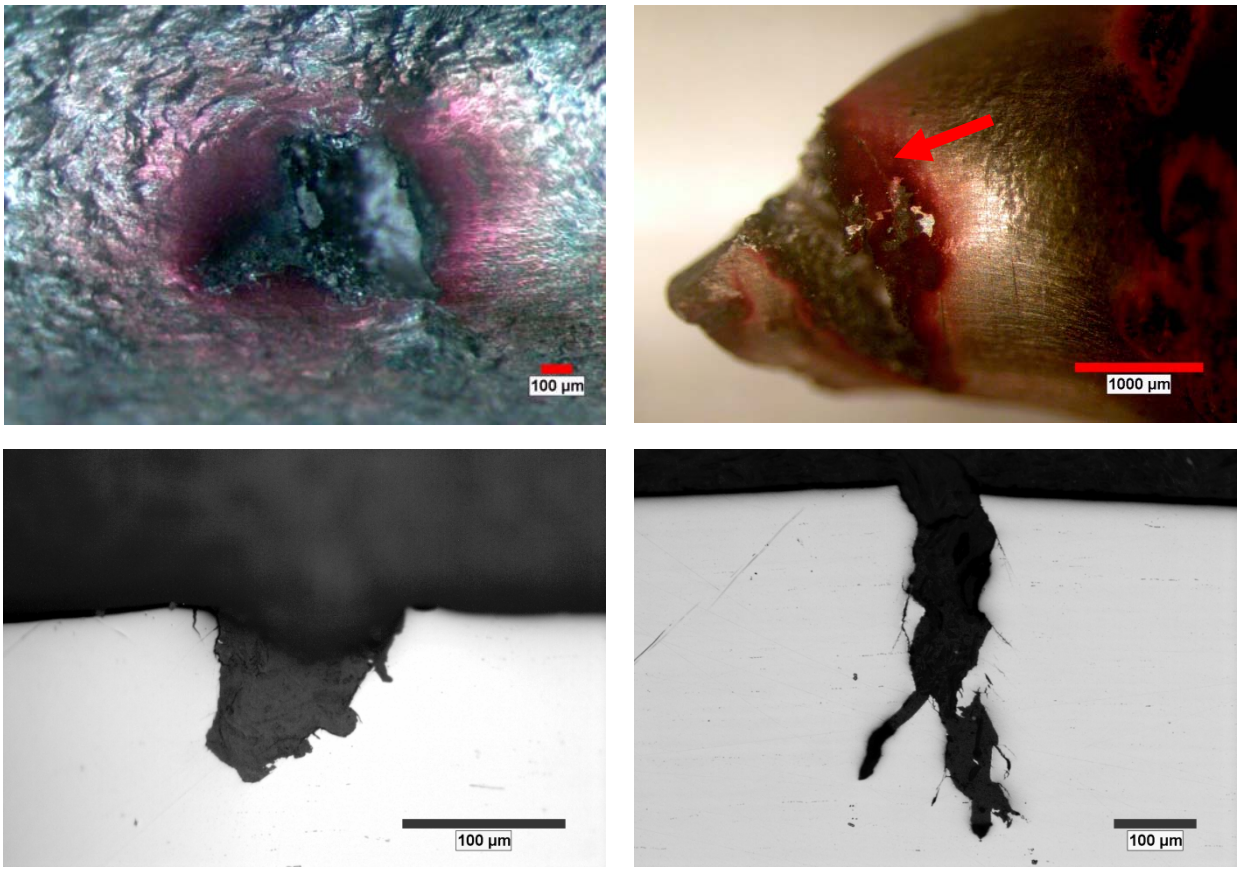

Low Cl^- (10 ppm) High Cl^- (30 ppm)

Figure 5.7: Impact of Cl^- on 316L tensile samples showing cross sections of the deepest cracks found along the sample surface. The test environments are detailed in Table 5.3.

Table 5.4: Environments and resulting crack density and velocity for 316L tensile samples evaluating Cl^- impact on stress corrosion cracking severity.

Sample	Water (vol%)	Cl^- (ppm)	pHe	Temperature (°C)	Pit Density (pits/mm)	Crack Velocity (mm/s)
Low Cl^-	60	10	5.8	200	0.04 +/- 0.05	7.09E-7
High Cl^-	60	30	5.8	200	0.31 +/- 0.04	9.38E-6

In the environments tested, the most severe SCC was seen in an environment with 60 volume% water at 220°C with 30 ppm Cl^- and pHe of 2.5. If the trends above hold true across the entire parameter ranges, then increasing the water further up to 90

volume% may increase SCC susceptibility of 316L stainless steel, as would increasing temperature, adding more Cl^-, or decreasing pHe.

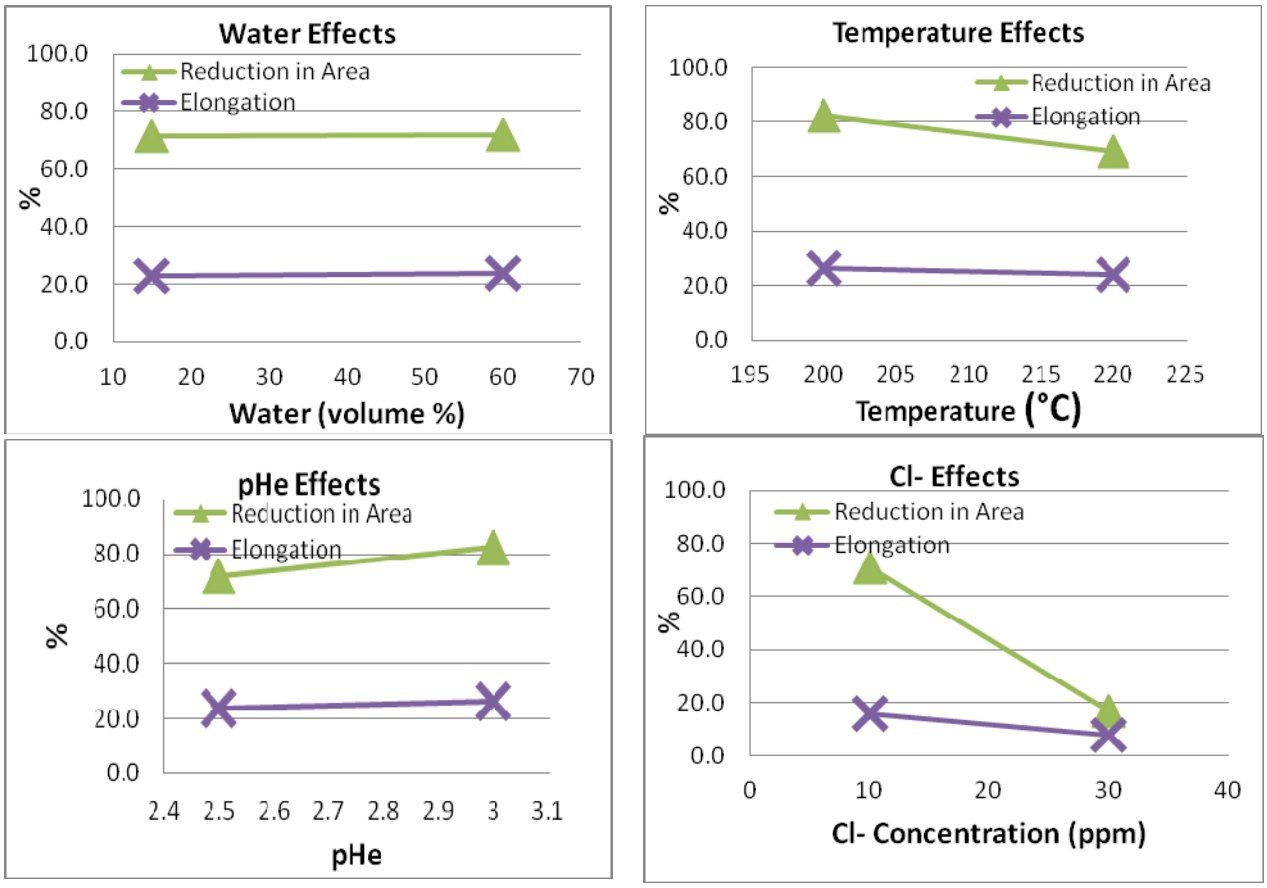

Figure 5.8: Impact of varying water, temperature, pHe, and Cl^- on % reduction in area and % elongation of 316L tensile samples.

The data in Figure 5.8 shows how varying each factor within tested range impacts the % reduction in area (%RA) and % elongation of the samples. Varying water content from 15 volume % to 60 volume % appears to have little to no affect on these variables, while varying temperature and pHe show some impact. As the test temperature increases from 200°C to 220°C, the % reduction in area and % elongation decreased, indicating a more severe environment. This supports the data presented earlier on crack density and velocity. Similarly, as pHe decreases from 3.1 to 2.5, SCC severity is seen to increase with a decreased % reduction in area and % elongation. Cl^- shows the most significant

impact on these variables, especially on % reduction in area. An increase in Cl- concentration in 60 volume % water solution from 10 ppm to 30 ppm decreased to % reduction in area from 71% to 17% when tested at 200°C. This indicates that cracking is likely initiating after yielding starts because the area does not start reducing until then.

5.3 Effect of Temperature and Water Content (for solutions with 0 ppm Cl^- and pHe = 3)

To better understand the effect of temperature and water content, a series of slow strain rate tests were conducted keeping Cl^- content constant at 0 ppm and pHe around 3 (ranging from 2.5-3.4). These two conditions were chosen based on the organosolv delignification environments found in Table 2.1 in which solutions do not contain added chlorides and typically contain acid. Since cracking was known to occur at a pHe of 3 it was chosen as the set values to better understand temperature and water effects given a condition known to cause SCC. The results from these studies can be seen in Figure 5.9.

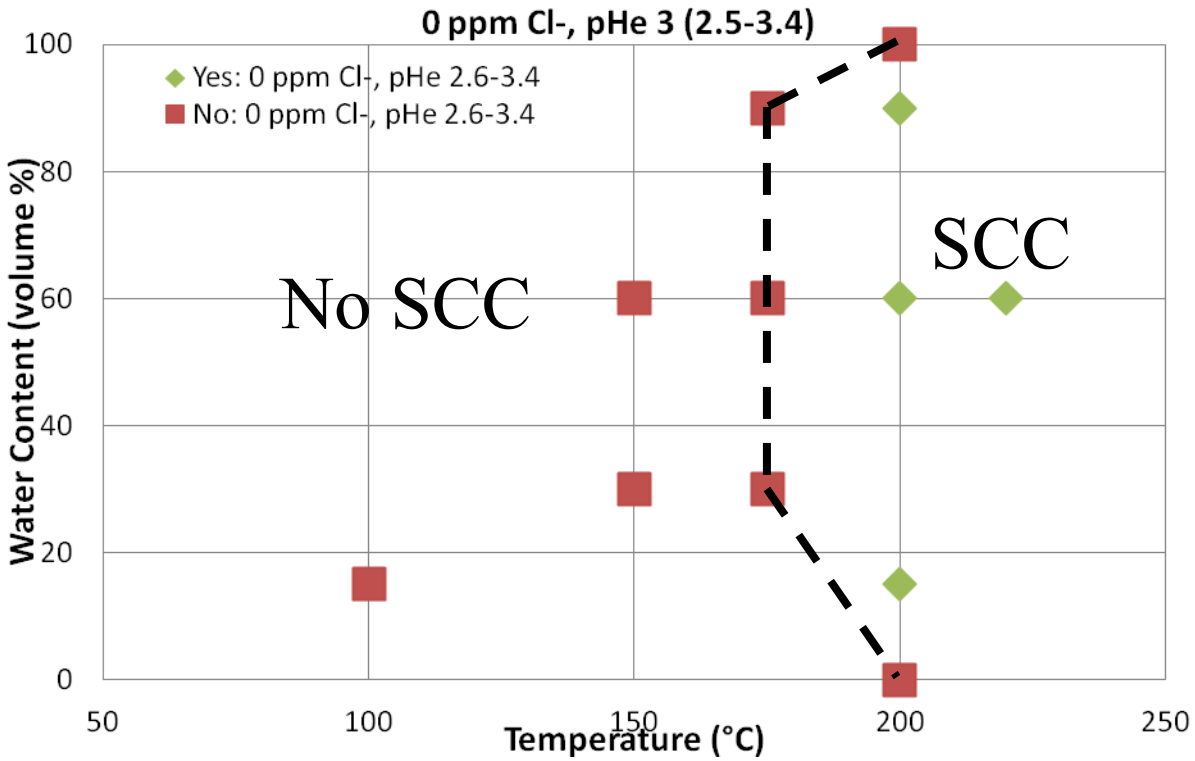

Figure 5.9: Stress corrosion cracking susceptibility for 0 ppm Cl-, pHe=3 environments with varying water contents and temperatures. Red squares indicate stress corrosion cracking did not occur and green diamonds indicate stress corrosion cracking occurred.

As expected the data follows the general trends in which SCC only occurs above 1 volume% water and at 200°C or above. It also shows that SCC only occurs in mixed ethanol-water environments. In acidic pure water or pure ethanol SCC did not occur, suggesting that for SCC a reaction needs to occur between the ethanol, water, and 316L surface that locally destabilizes the passive film. This reaction requires a minimum water content between 1 and 10 volume% water and SCC also does not occur above a maximum of ~90 volume% water. SCC of 316L stainless steel was only observed at elevated temperature, between 175-200°C and in the presence of acid.

5.4 Conclusions

The data from slow strain rate tests shown in Figures 5.1 to 5.10 indicates that SCC is possible in mixed ethanol/water environments at elevated temperatures. Threshold values for SCC of 316L stainless steel exist for temperature, water, pHe, and Cl^- content, and increasing the value of each variable above the threshold value show different impacts on crack density and crack velocity. Overall, crack velocity is more impacted by changing water content, pHe, and temperature. Cl^- most severely impact SCC by significantly increasing crack density and velocity. The crack morphology is also dependent on the environment. In acid/ethanol/water environments the cracks are carrot shaped and occur throughout the sample gage, but in Cl^-/ethanol/water environments the cracks are long and branched and only found in or near pits as seen in Figure 5.7. These pits are found throughout the gage length with at least one pit at the fracture surface.

Results show that as long as the organosolv delignification environment has the water or temperature below the threshold values and either the pHe above or Cl^- below the threshold then SCC is not likely. However, many of the environments satisfy both water and temperature threshold, so care needs to be taken to monitor pHe and Cl^- contamination to better understand SCC susceptibility.

This data indicates that cracking only occurs in the presence of acid and/or Cl^-, showing that one of these constituents is needed to destabilize the passive film and allow a crack to form. SCC initiation is likely an anodic process, especially in the case where pitting is associated with SCC. The SCC mechanism in water/ethanol solutions is most likely the mechanical process of anodic, film-induced cleavage process.

This information can also be used to determine the best organosolv delignification environmental parameters. Thus far, the environments have only been optimized for the delignification process, but if only minor adjustments are needed to ensure 316L could be used as equipment, costs could be minimized when compared to use of a more alloyed corrosion resistant steel. Alternatively, Table 2.1 indicates temperature ranges for some of the processes, like Alcell and Lignol. If the process is maintained at the low end of the range it is effectively below the SCC threshold, assuming no Cl- are present in the system. Already, the Alcell process is above pHe threshold, so would be less likely than the Lignol process to cause SCC of 316L. This information can be used to determine which organosolv delignification process would be the best to use in an industrial setting with 316L equipment.

CHAPTER 6

OVERVIEW AND FUTURE WORK RECOMMENDATIONS

6.1 Big Picture

The data clearly indicates that SCC is possible in ethanol/water environments containing acid or Cl^-. Before these environments are used industrially for organsolv delignification, more research needs to be done to further characterize the system. Until then, it is known that to prevent SCC pure ethanol could be used or very low water contents (approximately 1 volume %). Alternatively, the temperature could be maintained at or below 175°C to prevent SCC. Beyond controlling these two parameters, it is extremely important to prevent Cl^- contamination as Cl^- ions can destabilize the passive film. Very clean, inclusion-free 316L stainless steel could be used instead because the Cl^- ions typically rupture the film as localized anodes, such as MnS inclusions, on the sample surface. Finally, if the pHe is maintained above 4, SCC will also be less likely.

6.2 Future Work

This information has opened the door for further exploration in ethanol/water/acid/Cl^- environments, including:

1) Extended coupon exposures tests in these environments on the order of 15-30 days to better evaluate corrosion susceptibility and passive film stability.
2) Slow strain rate tests with electrochemical monitoring, including potential monitoring, current monitoring, and EIS, to monitor the surface and film behavior when a tensile force is applied to the sample.

3) An in-depth study of pit initiation as well as stress corrosion crack propagation, including interrupted slow strain rate tests to track where pits initiate and how cracks initiate from them and grow with time.
4) Further studies into water, temperature, pHe, and Cl^- effects on SCC susceptibility, looking for shifts in the trends caused by each variable as well as developing a better understanding of how the variables are interrelated, and when all three variables are being studied whether the pHe effect or Cl^- effect dominates.
5) Verification of the initial trends seen in the data by more testing at different set environments to see how the trends hold up to different base conditions.
6) Electrochemical and chemical analysis of surface film to understand the mixed solvent behavior and the possible chemical reactions occurring in the environment that may cause SCC.

REFERENCES

[1] M. Urquidi-Macdonald, D. D. Macdonald. Journal of the Electrochemical Society 136 (1989) 961-967.

[2] E. K. Pye. TAPPI Proceedings 1990 Pulping Conference 991-996.

[3] Maslen X. Pan, C. Arato, N. Gilkes, D. Gregg, W. Mabee, K. Pye, Z. Xiao, X. Zhang, J. Saddler. Biotechnology and Bioengineering 90 (2005) 473-481.

[4] C. Hongzhang, L. Liying. Bioresource Technology 98 (2007) 666-676.

[5] X. Pan, N. Gilkes, J. Kadla, K. Pye, S. Saka, D. Gregg, K. Ehara, D. Xie, D. Lam, J. Saddler. Biotechnology and Bioengineering 94 (2006) 851-861.

[6] M. A. Streicher. R. W. Revie, ed. Uhlig's Corrosion Handbook 2nd ed (2000) 601-650.

[7] Y. F. Cheng, J. Bullerwell, F. R. Steward. Electrochimica Acta 48 (2003) 1521-1530.

[8] A. J. Sedricks. R. H. Jones, ed. Stress-Corrosion Cracking Materials Performance and Evaluation (1992) 91-130.

[9] G. Gallo, J. Edmondson. NACE Corrosion 2008 Conference Paper No. 08555.

[10] J. Stewart, D. E. Williams. Corrosion Science 33 (1992) 457-474.

[11] J. E. Castle, R. Ke. Corrosion Science 30 (1990) 409-428.

[12] A. Pardo, M. C. Merino, A. E. Coy, F. Viejo, R. Arrabal, E. Matykina. Corrosion Science 50 (2008) 1796-1806.

[13] I. Toor, K. J. Park, N. Kwon. Journal of the Electrochemical Society 154 (2007) C494-C499.

[14] M. A. Baker, J. E. Castle. Corrosion Science 33 (1992) 1295-1312.

[15] M. A. Baker, J. E. Castle. Corrosion Science 34 (1993) 667-682.

[16] R. Chaves, I. Costa, H. G. deMelo, S. Wolynec. Electrochimica Acta 51 (2006) 1842-1846.

[17] B. Elsener, S. Virtanen, H. Boehni. Electrochimica Acta 32 (1987) 927-934.

[18] U. Lechner-Knoblauch, E. Heitz. Electrochimica Acta 32 (1987) 901-907.

[19] E. Heitz, C. Kyriazis. Industrial Engineering and Chemical Product Research Development 17 (1987) 37-41.

[20] Y. Marcus. Solvent Mixtures: Properties and Selective Solvation, Marcell Dekker, Inc.: New York (2002).

[21] S. Dixit, J. Crain, W. C. K. Poon, J. L. Finney, A. K. Soper. Letters to Nature 416 (2002) 829-832.

[22] S. A. Parke, G. G. Birch. Food Chemistry 67 (1999) 241-246.

[23] R. C. Newman. Corrosion 64 (2008) 819-823.

[24] G. M. Loudon. Organic Chemistry 4th ed, Oxford University Press: New York (2002).

[25] J. R. Chipperfield. Non-aqueous solvents, Oxford Science Publications: New York (1999).

[26] W. Koh, S. S. Jang, L. Goodman, P. M. Singh. Simulation study of the ethanol-water solution on the Fe2O3 surface. Project Review Meeting, July 19, 2011, Institute of Paper Science and Technology, Atlanta, GA.

[27] R. N. Parkins. Corrosion Science 20 (1980) 147-166.

[28] R. H. Jones, R. E. Ricker, R. H. Jones, ed. Stress-Corrosion Cracking Materials Performance and Evaluation (1992) 1-40.

[29] N. G. Thompson, J. H. Payer. DC Electrochemical Test Methods, NACE International, Houston, TX (1998).

[30] R. G. Buchheit. R. G. Kelly, J. R. Scully, D. W. Shoesmith, R. G. Buchheit, eds. Electrochemical Techniques in Corrosion Science and Engineering, Marcel Dekker, Inc.: New York (2003).

[31] EG&G Princeton Applied Research Basics of Electrochemical Impedance Spectroscopy (EIS), Note AC-1.

[32] A. J. Sedricks, B. C. Syrett, ed. Stress Corrosion Cracking Test Methods, NACE: Houston, TX (1990).

[33] V. K. Singh, V. B. Singh. Corrosion 43 (1987) 756-762.

[34] V. K. Singh, V. B. Singh. Corrosion Science 28 (1988) 385-395.

[35] S. Tajima, S. Komatsu, T. Momose. Corrosion Science 16 (1976) 191-193.

[36] I. Sekine, M. Yuasa, K. Kohara. Corrosion Science 31 (1990) 579-584.

[37] X. Lou, P. M. Singh. Corrosion Science 52 (2010) 2303-2315.

[38] A. J. Sedricks. Corrosion of Stainless Steels 2nd ed. John Wiley & Sons Inc.: New York (1996).

[39] C. V. Gopal Reddy, K. Kalyana, S. V. Manorama. International Journal of Inorganic Materials 2 (2000) 301-307.

[40] A. M. Bond, P. A. Lay. Journal of Electroanalytical Chemistry 199 (1986) 285-295.